Lignin derived nano-biocarbon: its deposition on polyurethane foam for wastewater dye adsorption and as a filler for composite applications

by

Curtis Seto

A thesis

presented to the University of Waterloo

in fulfillment of the

thesis requirement for the degree of

Master of Applied Science

in

Chemical Engineering

Waterloo, Ontario, Canada, 2021

Author’s Declaration

I hereby declare that I am the sole author of this thesis. This is a true copy of the thesis, including any required final revisions, as accepted by my examiners.

I understand that my thesis may be made electronically available to the public

Abstract

The use of natural biopolymers has seen a resurgence, due to their performance in natural organisms and biodegradable properties from an environmental perspective. As countries around the world continue to implement green policies, natural biopolymers will undoubtedly be a part of the solution that enables such a transition. Lignin is produced in large quantities as a by-product in lumber industries such as in pulping processes and has historically been only utilized in low-value applications, such as being burned for fuel. However, studies have shown that value-added applications for lignin can be developed due to its high carbon content, and high thermal stability. As such, the valorization and use of lignin has been the subject of extensive research.

In this thesis, research on the fabrication of lignin nanoparticles from pristine lignin (LN) and its modification via freeze-drying to produce nano-based freeze-dried lignins (NFLN) was investigated. LN and NFLNs were then carbonized to produce biocarbons. Characterization was performed on the LN and NFLN materials, prior to and after pyrolysis, with focus towards morphology and functionality. It was determined that the overall pre-treatment process imparted primarily a morphological change, and left the materials functionally similar as confirmed by Field Emission Scanning Electron Microscopy (FE-SEM), Fourier transform infrared (FTIR) spectroscopy, thermogravimetric analysis (TGA), elemental analysis and through analysis of the pyrolysis data.

The properties of the biocarbons demonstrated promising properties for use as a biobased carbon for material applications. The LN and NFLN biocarbons were deposited on to polyurethane (PU) foam to produce LN-PUs and NFLN-PUs. The cationic dye adsorption properties of biocarbon coated PUs were investigated using ultraviolet-visible spectroscopy (UV-vis) to determine removal efficiencies. It was found that at a dye concentration of 10 mg/L, the NFLN-

PUs removed more dye at 83.3% removal efficiency in comparison to the LN-PUs with 59.5% removal efficiency. This improvement in the performance of the NFLN biocarbons was attributed to the lower zeta potentials, indicating higher affinity for the adsorption of the positively charged dye. Furthermore, preliminary work into the use of LN biocarbon in composite applications was performed by incorporating it in natural rubber (NR) films. At loading levels of 5 and 10 phr, it was found that improvements in tensile and tear properties were observed, along with an increase in modulus. Overall, the use of LN and NFLN biocarbons show promise for use in adsorbent, coating, filler and pigment applications. Future work can involve the optimization of the described studies and be further extended to other polymer systems.

Acknowledgements

I would like to express my thanks to my two supervisors, Prof. Tizazu Mekonnen and Prof. Costas Tzoganakis, for the opportunity to conduct research in this Masters program. I thank you both for the advice, encouragement, guidance and support, of which I have found invaluable. I would also like to thank my other committee members, Prof. Hamed Shahsavan and Prof. Ting Tsui for their time and kind advice.

I am thankful for the financial support from Natural Resources Canada (NRCan) through the Clean Growth program.

I would like to express my gratitude to my colleagues, both past and present. I thank Dr. Boon Peng Chang for taking the time to impart his invaluable knowledge and experience. A special mention to Dylan Jubinville as well, for always being available to offer advice and assistance, which was of great help during my brief journey in academia. I would also like to thank the rest of my friends and colleagues: Dr. Arvind Gupta, Azin Adibi, Binh Minh Trinh, Ewomazino Ojogbo, Karelle Guaio, and Rohan Shorey, for their help and providing an enjoyable research environment.

A final thank you to my close friends and family, and a special mention to Belle Jiang for their love and encouragement. Also to Andrew Wong and Beemo for being supportive as well.

Table of Contents

List of Figures

List of Tables

Chapter 1: Introduction

1.1 Overview and Motivation

Polymer materials have been widely used over the course of human history. The first applications of natural biopolymers involved the usage of naturally found lignin-cellulosic materials such as wood and plant fibres. Over the past century, countless breakthroughs have been achieved in polymer science and engineering, providing more avenues to produce and implement synthetically produced polymers into consumer products. Nowadays, every facet of life has seen consumer products incorporating the use of synthetically produced polymers. Thus, synthetic polymers have proven to be commercially viable on a scale previously unheard of and the tailoring of properties for specific design applications is now commonplace.

More recently, some of the favorable properties of synthetic polymers have begun to be seen as a double-edged sword. Properties such as chemical or biological resistance to degradation which have enhanced the longevity of products also inadvertently result in disposal issues at the end of the product life cycle. Avenues for waste disposal are limited, as the majority of plastic wastes end up in landfills resulting in unsustainable accumulation of waste[1]. Recycling initiatives such as the reprocessing of waste polymeric materials[2] or burning for energy capture are limited in scale and are low-value applications. Overall, concerns have arisen regarding the use of synthetic polymers, stemming from the environmental impact of synthetic polymers due to their petroleum-based origins, and long-term depletion of fossil-fuels.

As environmental issues continue to have more pronounced effects on society, there is a growing need to implement policies and changes to minimize its damage. Thus, in order to mitigate these disadvantages and to transition towards environmentally sustainable practices, it is important to revisit the potential usability of renewable polymers. To combat these issues, countries have

begun to implement policies that promote environmentally friendly practices. One example includes Canada and various other G7 countries pledging to reuse, recycle or burn plastics by 2040. One potential solution is the usage of more environmentally friendly materials that can be biodegradable and possess lower carbon footprint, in contrast to many of the single-use plastics that are used today. As such, biomaterials including cellulose[3,4], lignin[5], starch[6] and wood have been the subject of extensive research due to their natural origins and abundance. Lignin in particular is projected to continue to grow in both global production capacity and commercial significance. There are over 300 billion tonnes of lignin present in the biosphere, making lignin a widely abundant and renewable material[7]. Most lignin is made commercially available as a by-product of the paper and pulp industry, with an estimated 70 million tonnes of lignin produced annually. Historically, only 2% of lignin were recovered and used for specialty applications, leaving the remainder to be burned as a low-value fuel, leaving much room for future valorization[8]. The use of lignin has been demonstrated in some commercial applications, such as in the production of carbon fiber, vanillin, or even as an additive, where it may be used as an adhesive, dispersant or surfactant[9]

Due to the high carbon and aromatic content of lignin, there is interest in exploring the its use as a precursor for carbonized products, as the weight yields of solid chars are higher compared to other biomasses[10,11]. Furthermore, as lignin is extracted from biomasses, its potential as a renewable source of carbon has been explored, for example as a substitute for petroleum-sourced carbon blacks[12]. Various pyrolysis studies have been performed using lignins as a precursor to various chars, with applications ranging anywhere from composite fillers[13] to activated carbons with high porosity for filtration[14,15] and other valorization purposes.

1.2 Research Objective

The research covered in this thesis entails the characterization and fabrication of lignin biocarbon. Further work is conducted to investigate the application of the biocarbon through its use as a filler in natural rubber composites, and as a nano-sized coating of polyurethane (PU) foam for dye adsorption.

The first section of the thesis investigates the fabrication of lignin nanoparticles via sonication and their respective pyrolysis into biocarbon. Lignin, being an abundant biopolymer with high aromaticity and carbon content, presents itself as an attractive precursor for biocarbon production. To that end, a pyrolysis experiment was designed to produce chars at a range of temperatures for both the lignin and the treated nanolignin. Characterization of the precursor and fabricated biocarbon is conducted to study the materials with respect to their functionality and morphology.

The second section of the thesis focuses on the application of the fabricated biocarbons as a filler of rubber composites, and as a nano-coating for polyurethane foam for dye adsorption applications. The overall goal of biocarbon incorporation into NR is to explore the feasibility of substituting the current dominating carbonaceous filler, carbon black, with a renewably sourced alternative. A second application is also explored, involving the use of lignin biocarbon as a coating on polyurethane foam to serve as an adsorbent for dye removal. Although various adsorbent materials have demonstrated good efficiencies at dye removal, the issue of recovering the adsorbent material itself can present a challenge. To that end, the immobilization of adsorbent material onto polymeric materials such as polyurethane foam could serve as an alternative solution. Furthermore, the polyurethane foams synthesized herein are based on an automotive flexible foam formulation, and thus may also explore the feasibility on the reuse of waste polyurethane foams.

The overall goal of the research is to explore the use of lignin biocarbon in various potential applications. Overall, the research discussed herein can benefit the environment through developing applications which involve the use of sustainable and renewably sourced materials.

1.3 Thesis Outline

There are five chapters to this thesis. The first chapter briefly discusses the motivation and objectives behind this research. The second chapter is a literature review to describe relevant background information on lignin, lignin nanoparticle fabrication, and pyrolysis. Further information is also provided regarding carbon-based applications in rubber composites, and as adsorbents for dye adsorption. Chapter three covers the experimental component of the research work, elaborating on the procedures and characterization techniques used for fabrication of lignin nanoparticles via sonication, and the production of biocarbons from the LN and NFLN lignins. The incorporation of biocarbons into natural rubber and PU foam are then explained. Chapter four covers the research results, going over all aspects regarding the fabrication of LN and NFLN biocarbons. The chapter ends by discussing research performed on their use in natural rubber films with the goal of enhancing the mechanical properties of the composite, and PU foam as a coating for dye adsorption for the removal of methylene blue. The last chapter summarizes the conclusions and recommendations of this work.

Chapter 2 Literature Review

2.1 Introduction to Lignin

Lignin is a biopolymer found within plants where it provides structural support by crosslinking the various polysaccharide components, thereby enhancing the mechanical strength of the cell walls. It is the second most abundant biopolymer, comprising of 15 – 36% of plant biomass[16]. Furthermore, its hydrophobic properties are used by vascular plants for water transportation. As a result of its antimicrobial properties, lignin is also deposited into wounds of plants to provide a barrier against pathogens[17].

Lignin as a material is an amorphous, complex polymer that is composed of three hydroxycinnamyl alcohol monomers: coniferyl, paracoumaryl and sinapyl alcohol as seen in Fig. 1[18,19]. These three lignin monomers, often dubbed monolignols, only differ in the degree of methoxylation on their aromatic rings. Monolignols are methoxylated and crosslinked through carbon-carbon, ester, and ether linkages in an enzyme-catalyzed process to further produce the phenylpropanoid units: guaiacyl, p-hydroxyphenyl and syringyl units during polymerization[19]. Owing to the complexity of the lignin molecule and its biosynthesis, a great deal of research has been conducted, studying the various mechanisms involved in its assembly. Monolignols are first constructed in the cytoplasm of plant cells[20], which are then transported to the cell wall at polymerization sites. Oxidative enzymes such as laccases[21] and peroxidases[22] facilitate the generation of lignin monomer radicals via dehydrogenation. These monomer radicals then undergo polymerization in a coupling reaction with other radicals on the free-phenolic ends of the lignin polymer chain[23]. It is interesting to note that the due to the complexity of its biosynthesis, the exact nature of lignin regarding whether its assembly was of a random or non-random nature was debated heavily in the past[24].

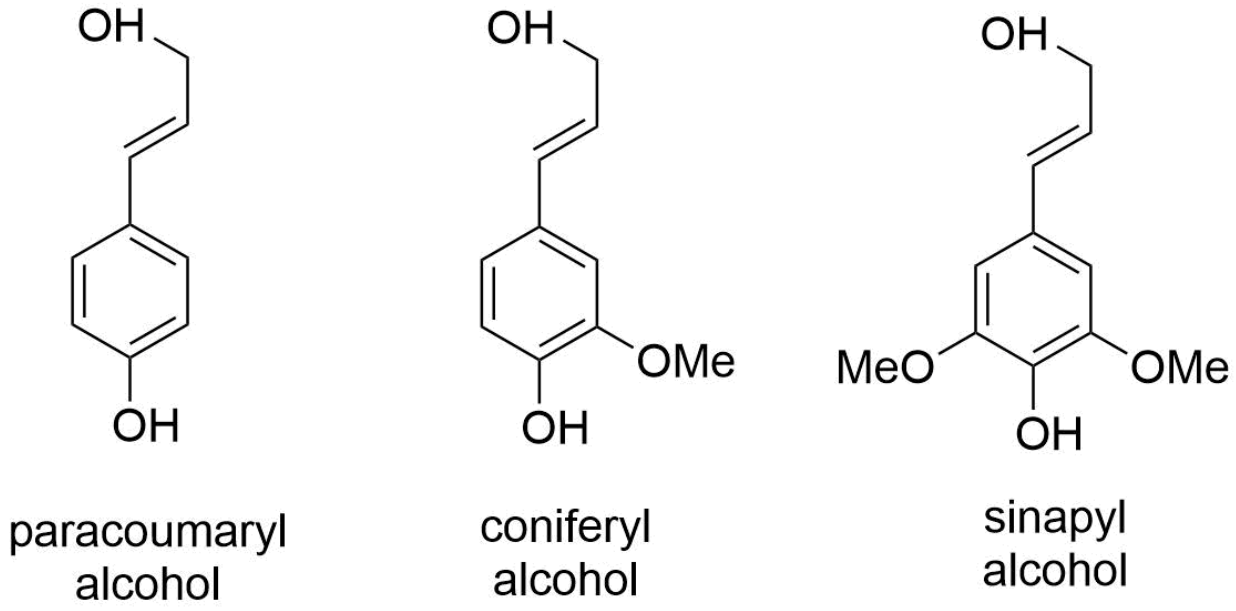

Fig 1. Lignin monomer units

Lignin can be classified into three categories depending on the source: angiosperms or hardwoods, gymnosperms or softwoods, and grass lignins. The composition of lignin differs among the different categories with respect to their phenylpropanoid contents. Hardwood lignins are sometimes referred to as guaiacyl-syringyl lignins due to their composition and comprise primarily of sinapyl alcohol[25]. Likewise, softwoods have been characterized as predominantly guaiacyl based and thus constructed predominantly of coniferyl alcohol, whereas grass lignins can contain a distribution of the three polymeric units[16]. The distribution of polymer units can result in different types of linkages occurring in lignin, and subsequently differing properties. Several types of linkages are present in lignin, some of which are shown in Fig. 2, such as the α-O-4, β-O-4, β-β, β-1, β-5, 5-5, and 4-O-5 linkages[19,26]. Of all the linkages, the β-O-4 is the most prevalent and the weakest of linkages. As a result, studies focusing on the depolymerization of lignin focus on the cleavage of this bond, via means including through pyrolysis, hydrolysis, enzymatic reactions or by treatment with ionic liquids[27]. The distribution of these linkages depends on lignin's

phenylpropanoid unit composition, which consequently affects the strength of the overall lignin polymer. In the case of softwood lignins, such as those sourced from coniferous trees, the higher guaiacyl compositions result in more β-5, 5-5 and 4-O-5 linkages, and thus can lead to higher chemical resistance of the overall lignin.

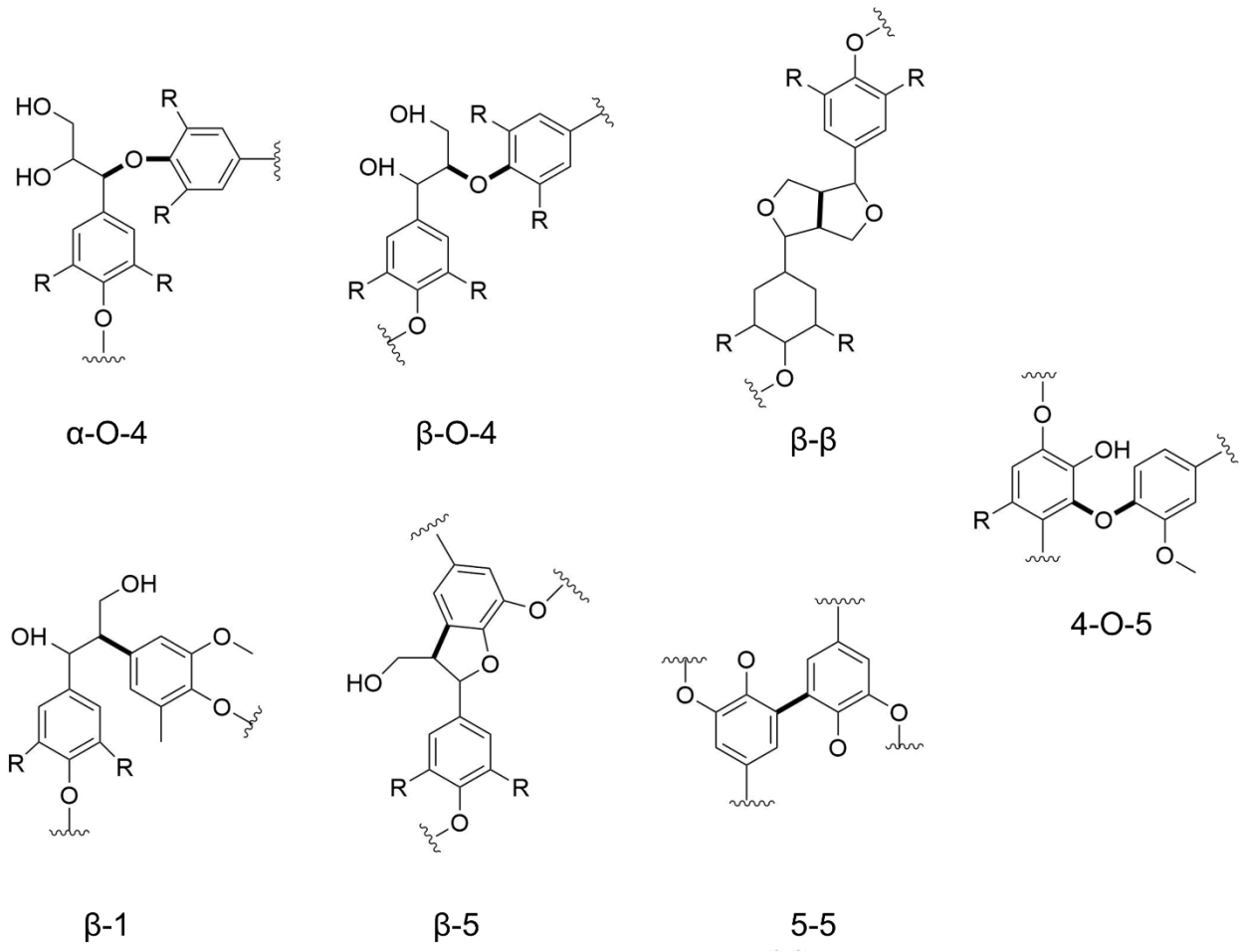

Fig 2. Major linkages present in lignin. Adapted from Diop et. al[27]

Overall, lignin polymer has a complex 3D structure that is difficult to fully characterize, rich in phenol and reactive hydroxyl functional groups. The extraction process can result in additional deviations in the lignin structure by imparting different functional groups onto the lignin structure. For example, some of these differences can be seen by variations in the elemental

compositions as shown for some lignins in Table 1. Further discrepancies can be caused by the source of biomass used for lignin extraction, resulting in different distributions of lignin polymer units. Consequently, it is pertinent to identify the type of lignin used when attempting to perform characterization.

Table 1. Elemental compositions and methoxyl contents of various lignins. Adapted from Mansouri et al[28].

	%C	%H	%N	%S	%O	%OCH_3
Kraft lignin	65.00	5.41	0.05	1.25	28.24	10.47
Calcium Lignosulfonate	44.84	5.15	0.02	5.85	44.14	8.70
Organosolv lignin	63.51	5.55	0.02	0.00	30.92	15.20
Soda lignin	65.00	6.12	0.17	0.00	28.64	19.30

2.2.1 Extraction processes (sulfur and sulfur-free)

Depending on the extraction process, a variety of different lignins can be produced. The basis of all lignin extraction processes first begins with the conversion of wood into fibrous materials. As the lignin macromolecule in its natural state is insoluble and crosslinked, further separation of the lignin is accomplished by the breaking of bonds, resulting in the formation of lignin fragments which can then be extracted using solvents. Lignins extracted as by-products from pulping processes are referred to as technical lignins, which can further be divided into sulfur or sulfur-free processes.

2.2.1.1 Kraft Lignin (Sulfate Process)

The term “Kraft”, meaning strength in German, is often used to refer to both the process and the produced lignin. The Kraft process which is also known as the sulfate pulping process,

produces Kraft lignin as a by-product and comprises up to 90% of global pulping processes[29]. In the Kraft process, lignins are separated from cellulose using white liquor, an aqueous solvent composed primarily of sodium hydroxide and sodium sulfide[16]. Kraft lignins are rich in hydrophobic aliphatic thiol groups.

In the Kraft process, sodium sulfide gets hydrolyzed and dissociates to form hydrosulfide ions which then proceeds to dissolve the lignin. This results in the formation of Kraft lignin with thiol groups or a "thiolignin", along with side products such as methyl mercaptan and methyl sulfide[16]. The delignification process with respect to the breakdown of linkages of the lignin molecule can be separated into three phases the initial, bulk and residual[30,31]. Delignification commences with the breaking of the phenolic α-O-4 and β-O-4 linkages. The next major reaction involves the breaking of non-phenolic β-O-4 linkages, followed eventually by the cleaving of carbon-carbon linkages and degradation of carbohydrates.

2.2.1.2 Lignosulfonates/Lignin from Sulfite Pulping (Sulfite Process)

A similar extraction method known as the sulfite process uses a sulfite pulping liquor, produced by passing sodium sulfite over a packed tower of limestone, magnesium oxide, ammonia solution or a caustic solution. Depending on the material used in the column, the produced liquor is referred to as either calcium, magnesium, ammonia or sodium based[16]. Usage of liquors sourced from different materials can also vary the pH of the sulfite pulping process, which generally occur in acidic or neutral conditions. Lignosulfonates characteristically have higher molecular weights and sulfur contents compared to Kraft lignins, due to the presence of sulfonic acid groups. These sulfonic groups result in hydrophilic properties and enhances water solubility[25].

Condensation, sulfonation and hydrolysis comprise of the primary reactions in the sulfite process. However, the reactions that occur can differ depending on the pH of the process. Under

acidic conditions, the loss of a hydroxyl group, or the cleavage of an α-ether linkage result in the formation of quinone methide intermediates. Sulfite ions can then be added onto the intermediates newly available α-site to form benzyl sulfonic acid units. Condensation reactions can also occur between the benzylic carbon and the carbon in the 6th position of another aromatic ring due to the formation of benzylic cations[32]. Under neutral conditions, sulfonation proceeds, but the presence of the α-sulfonic group's electron withdrawing effect results in a nucleophilic attack by another sulfite ion onto the β-position. This results in the cleavage of the β-aryl ether bond[32].

2.2.1.3 Other Lignins

A number of less-prevalent sulfur-free extraction processes exist, which can produce organosolv, soda, and hydrolysis lignin. The composition of sulfur-free lignins has a closer resemblance to lignin's natural state. The organosolv process is similar to traditional sulfur pulping processes, except that an organic solvent is used as a delignifying agent. Some commonly used solvents include formic acid, acetic acid, methanol and ethanol[33]. Organosolv lignin possess more phenol hydroxyls and carbonyl groups compared to sulfur-based lignins. Soda lignins are produced from soda-anthraquinone pulping processes, which largely resemble Kraft processes except for the sulfur-free liquor[34].

2.2.2 Lignin properties

As evidenced by the wide variety of available commercially extracted lignins, variability in properties exists. Nevertheless, the extracted lignins as a whole share a number of commonalities. Overall, research has demonstrated a multitude of lignin's beneficial properties due to its functional composition, including but not limited to its antioxidative, UV absorption, and antibacterial properties. Lignin is rich in hydroxyl and methoxyl groups that allow for the termination of oxidation reactions by hydrogen donation[5], allowing for its use as an antioxidant

such as in composite applications by operating with a radical-scavenging mechanism to protect the primary composite materials from degradation[35]. Furthermore, lignin itself has UV-absorption abilities, due the presence of UV chromaphores which are generated during its natural synthesis[5]. In addition to its antioxidative properties, lignin can be used as a preventative measure to eliminate the formation of radical species by absorption of UV light. Lignin also possesses antibacterial properties, stemming primarily from its phenolic double bonds in the α and β positions of the side chain, and a methyl group in the γ position[36]. Studies have been performed using solely lignin, and in conjunction with other antibacterial materials such as silver nanoparticles to provide a synergistic effect[37]. Lignin's antibacterial effectiveness is dependent on the conditions of the extraction process, as was demonstrated in a study by Nada et. al[38] using the Kraft process, which observed a decrease in antimicrobial activity with increasing processing temperature.

One of lignin's most appealing aspects is its sustainability as a renewable resource, due to its natural abundance in the biosphere. As a natural biopolymer, it is biodegradable, and its biodegradation has been shown to be facilitated by several microbial organisms. White-rot fungi are the principle organism that has been known to degrade lignin the most efficiently, and thus have been the most widely reported on[16,39]. The two categories of enzymes used by white-rot fungi are peroxidases and laccases. Owing to its complex, macromolecular structure, the specific mechanisms behind lignin biodegradation share the same complexity and have been the subject of much study in the past. Further elaboration on the mechanisms behind lignin biodegradation can be found in reviews on the subject[40].

2.2.3 Lignin Applications

Despite the Kraft process dominating the industry over the sulfite process for pulping, lignosulfonates currently make up the majority of commercial lignin applications. Global

lignosulfonate production in 2018 was estimated to be 1315 kilotons compared to 265 kilotons of Kraft lignin[41]. Of the sulfur-free lignins, hydrolysis and soda lignin are the only other lignins of commercial significance, but global annual production was estimated at only 5 kilotons.

Lignosulfonates are used in a wide variety of applications, such as in the construction industry where its demand is expected to grow[9]. Currently, a majority of lignosulfonates are used as a dispersant and concrete additive[42]. Another noteworthy application is its use in vanillin production, where until the 1990s, sulfite pulping liquors used to supply 60% of global vanillin demand[43]. This however was significantly diminished due to environmental issues in sulfite pulping, leading to a transition to Kraft pulping processes, where historically lignin supply was made less available due to its consumption as a low value fuel. Lignosulfonates have also demonstrated use as a dispersant, binder, adhesive, a stabilizer in colloidal suspensions or as an additive[9,44].

Although historically Kraft lignin applications have lagged behind lignosulfonate in terms of commercial significance, the shift towards Kraft pulping and commercial scale-up of Kraft lignin extraction continues to grow at increasing rates. Kraft lignin has been purposed for use in fertilizers, prerequisites for carbon fibers, binders and resins[9]. In addition, the conversion of Kraft lignin into lignosulfonates such as through acid sulfonation may also present itself as an alternative should the supply of lignosulfonates become bottlenecked, as currently the Kraft process dominates sulfite process in terms of pulping[44].

One of the most attractive proposals to produce significant value from lignins for involves their use as a precursors for carbon fibers, due to their significantly high carbon contents[45]. Lignins may also find use in the production of activated carbons[14], and carbon black substitutes[12,13]. Other

applications that may be developed include the depolymerization of lignin to produce raw materials for bioplastics and aromatic compounds[44].

2.3 Lignin nanoparticles

Research into nanoscale materials has been an area of high interest as of late, as the development of new engineered materials is required to support continued technological advancement. Much research has explored the applications of similar biopolymers on the nanoscale, such as cellulose. As a result lignin, being a similarly abundant and bio-compatible polymer, presents itself as an attractive alternative. Its properties may find use in a variety of applications such as in pharmaceuticals or cosmetics.

2.3.1 Lignin nanoparticle fabrication techniques

To date, several studies have been performed, demonstrating the ability to produce lignin nanoparticles, ranging from the use of homogenizers[46], ultrasonication[47], precipitation[48–50] and CO_2 saturation[51] techniques.

Table 2. Table summary of lignin nanoparticle techniques

Method	Particle Size Achieved	Reference
Homogenizer	< 100 nm	[46]
Ultrasonification	10 – 50 nm	[47]
Precipitation	40 – 500 nm	[48–50]
CO_2 saturation	35 nm	[51]

2.3.1.1 Homogenizers

Mechanical techniques employing the use of homogenizers to produce lignin nanoparticles has been reported. Nair et al.[46] produced Kraft lignin nanoparticles using a high shear homogenizer. In this experiment, mechanical homogenization was conducted for varying time durations. Homogenization conducted for 4 hours was able to bring down the particle size distributions to under 100 nm, with a average particle size of approximately 25 nm. Comparison between the unmodified Kraft lignin and sheared nanolignin molecular structures were performed using C-NMR and P-NMR. However, both techniques found no detectable structural changes within the lignin molecules.

2.3.1.2 Ultrasonication

Another simple method of producing lignin nanoparticles involves the use of ultrasonication. In this method, ultrasound waves result in cavitation, the rapid formation, growth and collapse of microbubbles. The occurrence of cavitation produces localized areas of extreme temperatures, pressures and high shearing forces[52–54]. These extreme conditions can result in the formation of radical species, and for polymers such as lignin, the homolytic scission of its polymer chain[55]. Using probe sonification, Gilca et al.[47] was able to reduce the size of an aqueous suspension of lignin with a size distribution of 1 – 10 μm to 10 – 50 nm. It was found that sonication of lignin did not result in significant changes to the lignin's composition or structure, save for degradation in certain lignin bonds.

2.3.1.3 Precipitation

Fabrication of lignin nanoparticles through chemical treatments have also been widely reported on and largely revolve around what has frequently been described as precipitation methods. Using this technique, particle sizes ranging from 100 – 500 nm[48,49] have been reported.

Experiments generally take advantage of lignin's solubility in solvents such as THF[49], and ethylene glycol[48,50]. An alternative approach to the precipitation technique involves exploiting lignin's additional solubility dependence on pH as lignins such as Kraft lignin and lignosulfonates can be solubilized in high pH solutions. One study produced lignin nanoparticles by dissolving a Kraft lignin into ethylene glycol, followed by slow acid addition to transition from a basic to acidic solution to induce a simultaneous pH and solvent change[48]. Dialysis further produces an aqueous solution of stable lignin nanoparticles. An alternative method employing the use of an acid-induced lignin precipitation technique can also be performed, whereby the initial lignin solution is brought to a high pH to solubilize the lignin. Precipitation into nanoparticles can then occur via slow acid addition.

A simple dialysis process can be conducted on lignin as well to produce nanoparticles. Rather than dropwise addition of an antisolvent, a semipermeable membrane can be used to gradually introduce an incompatible solvent such as water to induce the formation of nanoparticles. To date, a number of dialysis studies on nanoparticle fabrication have been reported, using solvents such as THF[49]. The introduction of the water causes the lignin to reorient its hydrophobic regions inwards into the forming nanoparticles. As with other techniques, nanoparticle morphologies tend to depend upon solvent selection and the method of fabrication employed. It was found that the use of THF produced spherical nanoparticles, whereas ethylene glycol produced more irregular morphologies, potentially as a consequence of solvent polarity and solvent exchange compatibility.

2.3.1.4 CO2 saturation

A precipitation with a compressed-fluid antisolvent (PCA) technique has been used to produce lignin nanoparticles. In this technique, a polymer solution is sprayed through an atomization nozzle, coaxially with a stream of CO_2. The mixing of CO_2 into the liquid droplets

results in a sudden volume expansion, greatly reducing the liquid's ability to solubilize the polymer and resulting in the formation of solid polymer particles. It was found that the particle size of the nanoparticles was dependent on the CO_2 temperature and pressure, solution flow rate and initial solution concentration. In the study that used PCA on Kraft lignin to produce nanoparticles, a mean particle size of 38 nm was achieved[51]. Further characterization was performed which identified the enhanced water solubility, UV absorption, and dispersion stability.

2.4 Carbonaceous materials and their applications

Carbonaceous materials have been used commercially in a wide range of applications, including primarily for mechanical reinforcement, and as a pigment due to its tinting strength[56–58]. Due to their inherent high carbon contents and structures, carbon nanofillers such as carbon black also possess high electrical conductivity[59] and the ability to improve thermal stability when compounded with polymers[60,61]. Carbon black currently remains the most widely produced and used nanofiller in formulations, being the only commercially feasible carbon filler produced on a large scale. In 2018, carbon black was estimated to have a market size of over 17 billion USD[62]. In comparison, an estimate in 2017 put carbon nanotubes at 2 billion USD, and graphenes at 35 million USD in a 2018 estimate. As can be seen, the commercial significance of other carbonaceous products is dwarfed by carbon black, but are expected to grow significantly as research into their development and applications continue.

Carbon black is a fine black powder of high purity carbon, produced from the incomplete combustion and thermal decomposition of petroleum products, such as natural gas, carbon rich oils, and various tars[63]. Carbon blacks are often described as aggregates of fused spherical primary particles, with low organic carbon content[64]. In its formation spherical particles grow from the deposition of elemental carbon, which fuses onto the growing particles.

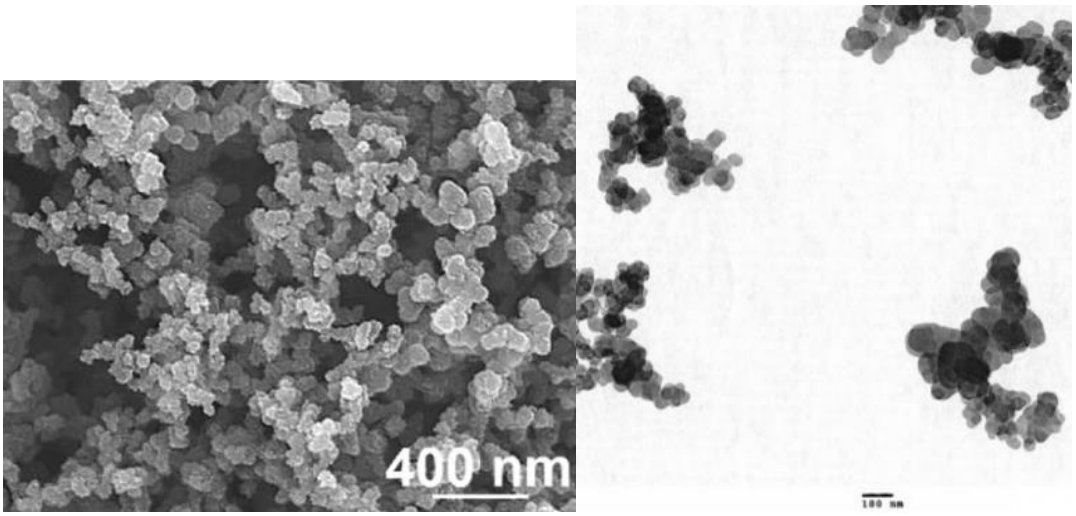

Fig. 3. Carbon black particles as seen by a) SEM[65] and b) TEM[66]

Carbon blacks have been reported to have good electrical conductivities, which has allowed its used in a great number of applications including in shielding of electrical cables, electronics in vehicles and in electrodes for fuel cells[59]. Due to the size of the carbon black industry, a number of carbon black grades are available. For applications requiring electrical conductivity, conductive-grade carbon blacks are used, which have been measured to have higher electrical conducitivites[67]. Furthermore, its use as a reinforcement in various elastomers is well known and has been widely reported on, such as its use in rubber tires. One of carbon black's first widespread commercial use was in rubber composites, due to carbon black's ability to greatly improve the abrasion resistance, while preserving their elastic properties[68].

Although work into other carbon materials has been extensively researched such as with carbon nanotubes (CNTs), multiwalled carbon nanotubes (MWCNTs), graphene and graphene oxides, their applications were historically limited to potential high-performance and cost areas due to a lack production at scale. Despite this, continuing research in the area of graphenes, and in particular graphene oxides, have demonstrated the ability for mass production and increasingly feasible conditions[69]. Furthermore, the production of advanced carbon materials such as graphene-

oxide-like materials using more environmentally friendly approaches has been investigated[70]. Nevertheless, the reported properties of various advanced carbonaceous materials have resulted in high interest in exploring their applications due to their remarkable range of properties, ranging from good electrical and thermal conductivities to high mechanical properties.

In contrast to the aforementioned carbonaceous materials, which are primarily sought for on the nanoscale size range, most other research on chars or biochars generally involve their use as micro or macro-sized particles. These applications include as a fertilizer[71], its use as an adsorbent for filtration[72], or as an additive in composite applications[73]. In soil, biochars can be introduced to adjust soil conditions, and supply nutrients due to its porous structure and surface area. Other soil properties can also be adjusted, such as with the pH levels of soil which has been correlated to the bioavailability of nutrients[71]. With respect to the use of biochar as an adsorbent, the key properties that must be optimized are its porosity and surface area. To that end, chars produced for this application generally undergo higher pyrolysis temperatures, in addition to undergoing activation treatments to further develop porous structures. In the case of biochars, the selection of biomass can also be a significant factor due to the tendency for biochars to resemble their original biomass structures[74,75]. A number of different biomasses have been used as precursors for high surface area biochars, such as seaweed[72], sawdust[76]. Some current sources used to produce activated carbon on a commercial scale include coal, coconut shells and wood.

2.4.1 Carbonaceous adsorbents for dye adsorption

Dyes are used in significant quantities in a number of industries such as in textiles, food, cosmetics and paints. As dyes are known to cause health issues if left in wastewater, the removal of dye from industrial wastes produced from these processes is a significant environmental and health concern. In the case of methylene blue, the health effects are not as pronounced but may

still include diarrhea, inflammation, nausea and vomiting[77,78]. Techniques including but not limited to biological treatment[79], membrane filtration[80], and photocatalytic degradation[81] have been used to treat dye wastewater. Among the different techniques, adsorption is considered the most prevalent as its simplicity suggests ease in scaling up, combined with the general low cost and high efficacies of the adsorbent materials. A wide range of materials have been used as adsorbents such as clay, alumina, and various carbonaceous materials[78,82].

2.4.1.1 Deposition of carbon-based adsorbents onto foam

The implementation and removal of the adsorbent material itself can present a challenge. For instance, the direct usage of powder-like adsorbent materials can consequently become environmental hazards if not filtered or properly removed. Techniques involving the immobilization of adsorbent materials, such as its incorporation into membrane materials and polymeric materials can address these issues. In particular, research into the coating of polyurethane (PU) with various carbonaceous materials such as activated biocarbon[83], carbon nanotubes[83] and soot[84] has demonstrated the ability to adsorb dye while facilitating for the recovery of adsorbent material, as opposed to using the adsorbents directly. PU foams possess a range of appealing properties, with its high surface area to volume ratios, and the presence of both polar and non-polar functional groups lending it versatility in adsorption applications. Furthermore, the generation of PU waste is also a concern as PU production continues to grow, a portion of which is attributed to foams[85]. Current recycling applications include low-value applications such as its use in energy recovery via burning, or as a filler in composites[86]. The preliminary work herein briefly describes the use of a PU foam formulation that mimics the composition and properties of commercial automotive flexible foam, and thus may present an alternative value-added application for PU waste.

2.4.2 Carbonaceous fillers for rubber composites

Rubbers are elastomers, possessing viscoelastic properties that have low elastic modulus and high failure strain. Due to their unique properties, rubbers have played an important role in producing various goods and applications. The first rubbers used and documented in history were natural rubber (NR), which can be naturally extracted from various angiosperms in the form of a sap or latex, a stable dispersion of rubber microparticles. Although a number of species are known to produce latexes, the most common source is the Hevea brasiliensis tree, which produces a majority of commercial natural rubber, otherwise known as cis-1,4-poly(isoprene)[87]. Not long after its scientific discovery, synthetic polymers were synthesized from petroleum by-products with different, and in some cases superior properties, with some of the most prevalent synthetic rubbers including styrene-butadiene rubber (SBR) and nitrile rubber. The viscoelastic properties of rubber have resulted in extensive societal use, ranging from all sorts of commercial and industrial applications.

Furthermore, fillers can be added to rubber formulations to provide enhanced mechanical, thermal and conductive properties, depending on the selection of filler. To that end, a great number of different types of fillers have been researched, ranging from sustainable biopolymers[3,88] to clays[89]. Carbonaceous fillers are a category of fillers that have been used on a commercial scale, and have been the subject of extensive research. In fact, the most widely used filler in the rubber industry is carbon black, where it is used as a pigment and for reinforcement. Carbon black is commonly used in all sorts of composite applications, such as with SBR for tires. The use of other advanced carbon-based materials in rubbers have been researched, including carbon nanotubes[90–92], and graphenes[93]. With growing interest towards using renewable fillers, biobased carbon materials, or biocarbons, have also been extensively studied

and used to produce rubber composites. To date, a wide range of different biomasses such as rice bran[94], lignin[13], wood[95], chitin[96], and nanocellulose[97] have been used to produce biocarbons to be used with various rubbers.

2.5 Lignin pyrolysis for biocarbon

Due to the high carbon and aromatic content of lignin, there is interest in examining the usage of lignin as a precursor for carbonized products, as the weight yields of solid chars are higher compared to other biomasses such as cellulose and hemicellulose[10,11]. Furthermore, as lignin is sourced from biomasses, its potential as a renewable source of carbon is an appealing aspect and may be used for example as a substitute for petroleum-sourced carbon blacks[12]. To that end, lignin has been used in various experiments to produce biobased carbons for a number of different applications, with the goal of substituting existing carbonaceous products with a more renewable and sustainable alternative. These applications have ranged from lignin biochar's use as an additive in simple applications as a filler, as an adsorbent, and even as a precursor for lignin-based carbon fibers.

Lignin has been used in a number of studies, exploring its use of as a carbon black substitute after carbonization. The studies generally involve the ball milling of carbonized lignins, followed by the characterization of their properties at different temperatures[12,13]. By virtue of the lignin biochar's high carbon content, ranging from 84 – 90%, the biochars have been evaluated to be a suitable replacement for carbon black. For a comparison, some carbon blacks have been found to have a carbon content of 97% or above[64], but carbon contents for lignin biochar on the higher end can be achieved as evidenced by the correlation between higher pyrolysis temperatures and increasing carbon content. Additional work has been performed in the use of lignin biochar as an additive in polymers such as styrene-butadiene rubber[13] (SBR) and polytrimethylene

terephthalate[98] (PTT). Overall, the addition of lignin biochar into polymers resulted in mechanical improvement on par with carbon black, or alternative conventional fillers such as glass gibers or minerals within the micron-sized range.

Similarly, the production of highly porous, high-purity carbon materials known as activated carbons is a well-established industry. Lignin pyrolyzed at high temperatures 900 °C or above have been reported to produce highly-porous materials and thus could be suitable for these applications[12]. Other studies have shown that the morphology and surface areas can be further tuned by treatment of the lignin through either freeze-drying[99] or with the additions of additives[100]. A study by Chen et al.[99] involved the freeze-drying of lignin at low concentrations, followed by pyrolysis at 1000 °C was able to produce carbonized lignin with high surface area of 702 m^2/g. In a study by Gonugunta et al.[100], the addition of 15% KOH the lignin followed by freeze drying prior to pyrolysis was reported to produce char with a porous microstructure. As surface area is one of the primary factors lending to good adsorption capabilities, there is promise in exploring lignins use as a carbonized precursor to produce renewable adsorbents.

Research into the development of lignin-based carbon fibers has been ongoing, from which a number of factors have been found to be relevant to the production of carbon fiber. The source of the biomass, whether it was sourced from hardwoods or softwoods, molecular weight distribution, and processing conditions require optimization[45]. Although there are extensive efforts into the commercialization of lignin carbon fibers, there are a number of existing obstacles, ranging from the inconsistency of the lignin sources, and optimization of both the lignin properties and processing. Despite these obstacles, pursuing lignin-based carbon fibers remain an attractive prospect from both a commercial and environmental standpoint. For example, the cost of lignin as a raw material is estimated to be a fraction in comparison to polyacrylonitrile (PAN), an example

of a conventional carbon fiber precursor material[101]. In addition, the overall process to produce lignin-based carbon fibers has been estimated to produce 22% less greenhouse gas emissions[102].

Overall, as the lignin industry continues to grow with improvements in availability and consistency, the commercial feasibility of lignin as a precursor for various carbonaceous products will grow in parallel.

2.5.1 Pyrolysis mechanism of lignin

The pyrolysis of a biomass results in the formation of char, an aromatic polycyclic structure that is more thermally stable. A number of products such as water and various incondensable gases are produced from this process. Char formation can be divided into two primary processes: depolymerization and fragmentation[10]. In depolymerization, the linkages between monomer units are broken. The degree of polymerization is reduced until the molecules are volatilized, and some of the products may remain in the liquid product, tar. Fragmentation on the other hand occurs in the covalent bonds of both the polymer and within the monomer units. This process produces incondensable gases and condensable small chain organic compounds. In addition to these primary processes, secondary reactions may occur as a result of the presence volatile products: cracking and recombination. Cracking involves solely the volatile products, which may undergo further breakdown of their chemical bonds, resulting in the production of lower molecular weight products. In recombination, higher molecular weight products are produced from the volatiles, and in some cases a secondary char may be produced[103]. Polycyclic aromatic hydrocarbons have been found to promote recombination reactions. These secondary reactions can be catalyzed at various sites, including the char surface, catalysts, or the reactor surface.

Two primary factors affect the formation of char: the temperature and heating rate. It is known that slower heating rates promote more char formation and reduce the production of

volatiles. Through a large number of studies and reviews[10] on the degradation of lignins, and similar materials such as cellulose and hemicellulose have been investigated. A brief summary of the degradation pathway of lignin is presented in Fig. 4.

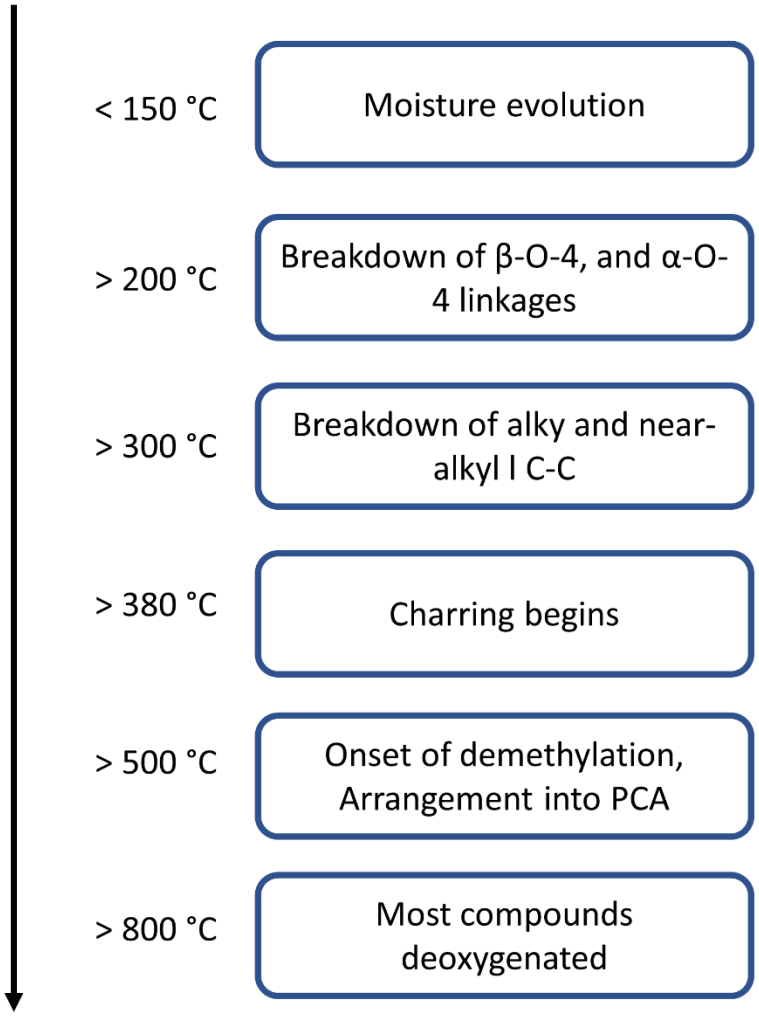

Fig. 4. Summary of lignin degradation with respect to temperature.

Similar to cellulose, and hemicellulose, thermograms of lignin establish that moisture removal is the sole significant occurrence under 150 °C. Above 200 C, the weakest of the ether linkages begin to degrade, starting with the α-O-4 linkage. The β-O-4 linkage, the most prevalent and easily cleaved linkage found in lignin, can start degrading at 245 °C. The removal of these

linkages results in the release of CO, CO_2, H_2O, and phenolic compounds that resemble the structure of lignin monomers. At temperatures above 300 °C, carbon-carbon bonds can start to break. This results in the evolution of compounds with 1-3 carbon atoms, such as methane, acetaldehyde, acetic acid, and further phenolic compounds. The highest rate of lignin decomposition, and subsequently highest rate of phenol production, is found between the range of 360 – 400 °C. The charring process initiates at 380 °C, starting with the fragmentation reaction, where methoxy groups can be substituted with -OH, $-CH_3$, or -H groups. Methanol, and methane at 430 °C, is produced as a byproduct of the fragmentation of methoxy groups. At 450 °C, a majority of the initial lignin monomer linkages are no longer present, save for the phenyl 5-5 and ether 4-O-5 linkages. This is followed by the disappearance of $-CH_3$ groups, or demethylation, occurring between 500 – 600 °C. At 800 °C, it is expected that the char is mostly deoxygenated.

2.5.2 Effect of pyrolysis conditions on char

The selection of pyrolysis conditions is important, in order to optimize yields and properties of the targeted product. In particular, the effect of the temperature and heating rate on the pyrolysis of various biomasses with respect to char yield have been extensively studied in the past. Higher temperatures result in an increase in carbon content of the char, or carbonization, and the reduction of functional groups. At sufficiently high temperatures and with appropriate selection of the biomass, extremely high temperatures result in essentially elemental carbon. Furthermore, the development of structures such as graphitic carbon can occur[104]. Pyrolysis procedures where the aim is for the gasification of the biomass generally involve fast heating rates such as those above 100 °C/min, whereas if carbonaceous products are sought, the opposite is true[105,106]. Two examples are presented in Fig. 5a and 5b in studies performed on wood[106], and cellulose[107], where in both instances, a substantial difference in char yield are observed. In the study performed by

Dall'Ora et al.[106] on wood, char yields of as low as 1 – 6 % were obtained at heating rates of 10^4 – 10^5 K/s, in comparison to 15 – 17 % at 10 – 20 K/min. It is suggested that the slower heating rates provides the biomass sufficient residence time to undergo dehydration reactions, which leaves behind a skeleton rich in double bonds and aromatic structures that is conducive to the formation of char[108]. In the case of cellulose, it has been shown that at lower temperatures, dehydration reactions dominate over depolymerization[107].

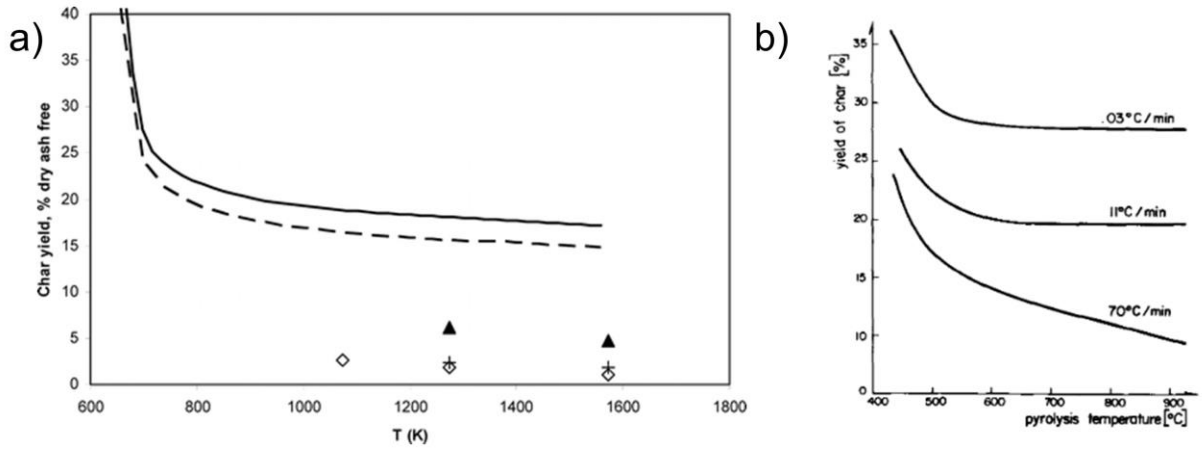

Fig 5. Effect of heating rate on the char yield of (a) wood[106] and (b) cellulose[107]. In figure (a), individual symbols represent pyrolysis of wood samples at fast heating rates, and lines at heating rates of 20 K/min.

Although lignin shares a similar trend with reducing char yields at higher heating rates, studies have shown the effect within a smaller range of heating rates of 5 – 20 °C/min may have a less pronounced effect in comparison to biomasses such as wood and cellulose (Fig. 6).

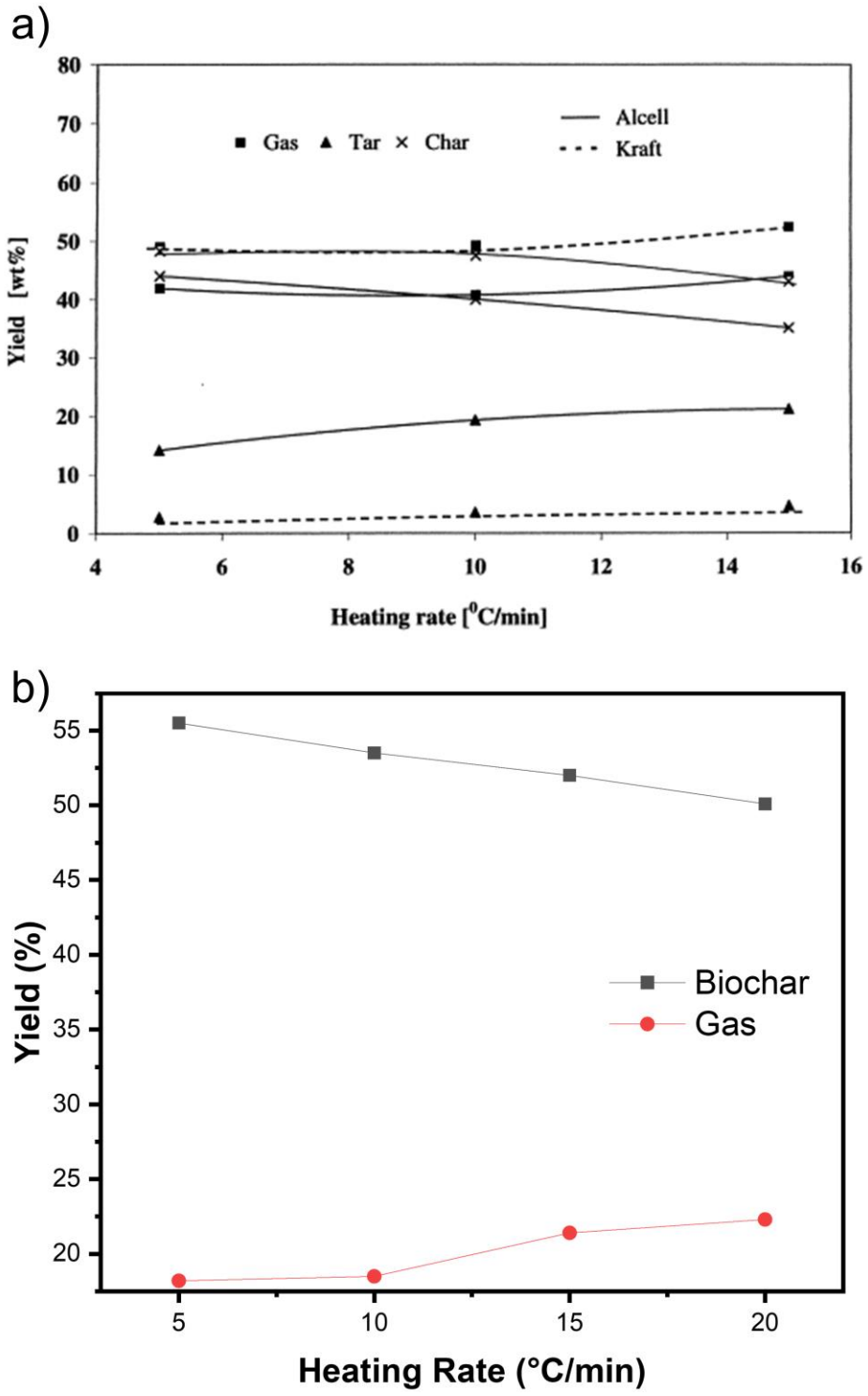

Fig. 6. Pyrolysis yield of products from lignin at different heating rates: (a) 5 – 15 °C/min[109] and (b) 5 – 20 °C/min (Adapted from Li et al.[110]).

Chapter 3 Materials and methods

3.1 Materials

Dealkaline lignin powder (L0045), which is sodium lignosulfonate modified by the manufacturer through partial desulfonation, oxidation, hydrolysis and demethylation, was purchased from TCI chemicals. For pyrolysis experiments, this powder was dried at 105 °C overnight to remove moisture. Dimethyl sulfoxide (DMSO) was purchased from Sigma Aldrich. Polyol (ethylene oxide capped polyether triol), surfactant (Tegostab® B8870), and catalyst (triethylenediamine in dipropylene glycol) were obtained from Monument Chemicals (USA), Evonik (USA), Air Products (USA), respectively. Diphenylmethane diisocyanate (MDI) and analytical grade methylene blue (MB) dye were purchased from Sigma-Aldrich.

For the preparation of natural rubber composites, natural rubber latex with a solids content of 60 wt% was purchased from Chemionics Corporation, OH, USA. Pelletized 85% potassium hydroxide (KOH), 99% zinc oxide (ZnO) powder were purchased from Sigma-Aldrich, USA. 99.5% sulfur and 98% zinc(II) dibutyl dithiocarbamate (ZDBC) were purchased from Acros Organics and Fisher Scientific, Inc., Canada respectively.

3.2 Lignin nanoparticle fabrication

2.5 g of untreated lignin (LN) powder was first dispersed in 50 mL water and sonicated to produce lignin nanoparticle dispersion. The dispersion was then sonicated for up to 2 hours, with particle size measurements conducted to monitor changes in particle size. A Fisher Scientific model 120 sonic dismembrator with a max frequency of 20 kHz and a 3.175 mm (⅛”) probe was used for the sonication. The sonication was performed in pulse mode by alternating between a 30 second ultrasound cycle followed by 10 seconds of no ultrasound. The aqueous lignin nanoparticle

solutions were then freeze dried until the NFLNs remained. A similar method was used to fabricate lignin nanoparticles from lignin extracted from an alkaline process as reported by Gilca et al.17. The lignin nanoparticle dispersion was then freeze dried to obtain dried lignin nanoparticles (NFLN).

3.3 Pyrolysis of LN and NFLN

To pyrolyze the dried lignin, LN and NFLN samples were held using a quartz boat and placed into a quartz tube. The tube was sealed with a flange for use in a Lindberg/Blue M Mini-Mite^{TM} tube furnace and a continuous flow of N_2 gas was applied to purge the tube of residual air. For each pyrolysis run, a temperature ramp rate of 10 °C/min was used. Temperature setpoints of 600, 750, 900 and 1050 °C were employed for their respective runs and held for 6 hours. Upon completion, the tube and flange setup were allowed to cool to room temperature, and the quartz boat was taken out to recover the pyrolyzed lignin biocarbon. The overall sonication and drying treatment, along with the carbonization procedure is shown in Fig. 7.

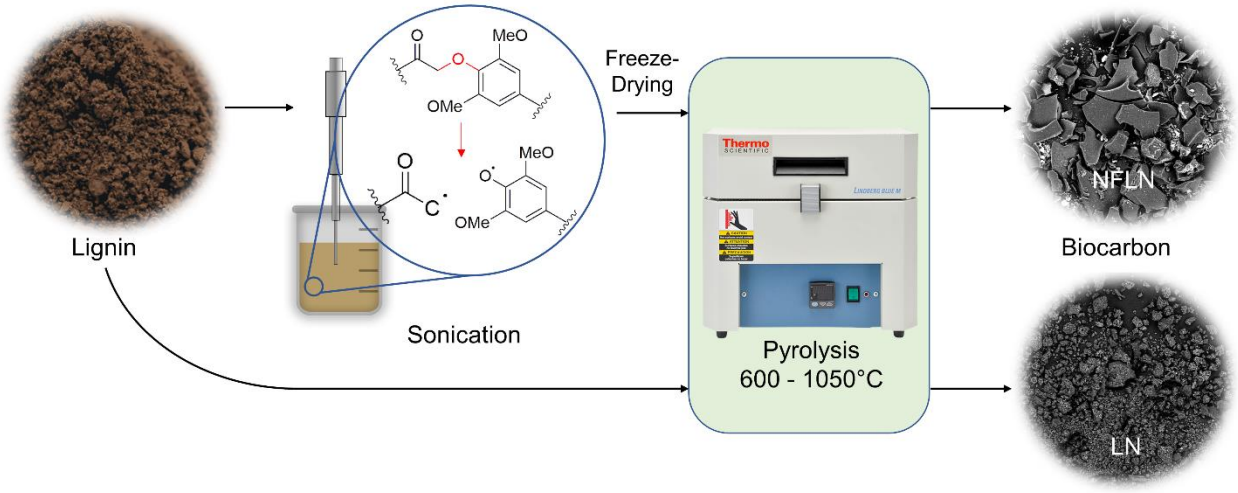

Fig. 7. Lignin and nano-lignin through sonication and freeze-drying treatment, followed by carbonization into biocarbons at different temperatures.

3.4 Characterization

3.4.1 Structural characterization of LN and NFLNs

The particle size distributions of lignin particles dispersed in water were obtained using a Zetasizer (Nano ZS90). Samples for the measurement were prepared by dispersing the particles in deionized water at a concentration of 0.1 wt.% to obtain the average particle size (D50) and distribution. The Zetasizer was also used to evaluate the weight-average molecular weight of lignins dissolved in DMSO, using a static light scattering function. A reported refractive index increment (dn/dc) for sodium lignosulfonate in DMSO of 0.117 was employed for the calculations[111].

A Zeiss Leo 1530 Field Emission Scanning Electron Microscope (FESEM) was used to observe structural changes in the precursor LN and NFLN in comparison to their respective carbonization states. For each sample, the solid powder was pressed against a carbon tape covered stub with loose particles removed using pressurized air. Energy-dispersive X-ray (EDX) mapping was also carried out to analyze carbon, oxygen, sodium, and sulfur elements on the sample surface.

3.4.2 Elemental analysis

Elemental analysis was conducted using a Costech Elemental Analyzer 4010 (Costech Analytical Inc., Italy) for carbon, nitrogen and sulfur. An Elementar Pyrocube Elemental Analyzer (Elementar, Germany) was used to determine oxygen content.

3.4.3 Fourier transform infrared (FTIR) spectroscopy

The infrared (IR) spectra of all materials were obtained using a Thermo Scientific Nicolet 6700 Fourier Transform Infrared (FTIR) spectrometer. Sample pellets were prepared by grinding 1 mg of the sample powder with 200 mg of potassium bromide (KBr) using a pestle and mortar,

and then pressed into a pellet. FTIR scans were then conducted in transmittance mode between 500 and 4000 cm^{-1} for 32 scans.

3.4.4 X-ray diffraction (XRD)

A Bruker D8 Discover X-ray diffractometer using Cu-K α as a radiation source was used to observe the change in crystallinity and ordering. Powder samples were placed onto the surface of the circular cavity sample holders and diffraction angles (2θ) were recorded between 2.5 to 70°.

3.4.5 Surface area analysis

For the surface area analysis, the pyrolyzed biocarbons were degassed under nitrogen gas at 180 °C for 1 hour, and the baseline lignins at a lower temperature of 105 °C for 6 hours. The surface area of the samples prepared as such was then determined using a Micromeritics Gemini VII 2390 Surface Area Analyzer employing the Brunauer-Emmett-Teller (BET) method.

3.4.6 Thermogravimetric analysis (TGA)

A Mettler Toledo TGA 2 (Mettler Toledo, USA) was used to conduct a thermogravimetric analysis (TGA) of the lignins. 10 – 20 mg of sample was used for each analysis. For each run, the temperature initialized and held at 115 °C for 10 minutes to remove moisture, followed by heating to a temperature of 1050 °C at 10 °C/min in nitrogen gas.

3.4.7 Raman Spectroscopy

Raman spectra were obtained using a Bruker Sentarra Raman spectrometer with a wavelength of 532 nm and an output power of 10 mW as an excitation source. Raman spectra were collected from 70 to 3000 cm^{-1} with an integration time of 10s. A baseline correction was performed to analyze the 900 – 1800 cm^{-1} region for deconvolution using OriginPro 2020 software. Deconvolution was performed using the Peak Analyzer's Fit Peaks (Pro) function.

3.5 Preparation of biocarbon and natural rubber films

NR films containing 0, 5 and 10 phr of LN biocarbon filler were produced using a film casting method and the NR formulations are shown in Table 3. All of the additives, except for the LN biocarbon and NR latex, were first dispersed into a vial containing 10 mL water using the Fisher Scientific model 120 sonic dismembrator. Prior to use in the composites, both chars were first subjected to ball milling using a Classic Line Fritsch Pulverisette 7. For the films containing LN biocarbon, the ball milled LN biocarbons were predispersed into another vial containing 10 mL water using the probe sonicator. Both vials of additives and LN biocarbon were then poured into a beaker containing the NR latex and stirred. The final mixture was then poured into moulds and allowed to dry for 1-2 days. The films were then gently peeled off the moulds and cured in an oven at 100°C for 1 hour to complete the crosslinking of the rubber.

These films were used for tensile and tear mechanical property testing. Tensile tests were conducted in accordance with ASTM D882-18, using a Type V specimen (ASTM D638-14) with a 500 mm/min strain rate. The tensile strength, modulus at 50, 300 and 500% were reported. Tear tests were conducted in accordance with ATM D624-12 with modified sample dimensions using a strain rate of 50 mm/min. Die T specimens of 4 x 2 cm (length x width) with a 2 cm tear initiation were prepared. For both tensile and tear tests, five samples were tested using an AGS-X Shimadzu universal testing machine with 5 kN load cell.

Table 3. Composition of Natural Rubber formulations

Material	Parts Per Hundred (phr)
Natural rubber latex	100
LN biocarbon	0, 5, 10
3% KOH solution	1.5

Sulfur	1.5
ZDBC	0.7
ZnO	1.3

3.5 Fabrication of polyurethane and deposition of biocarbon

Polyurethane (PU) foam was prepared by blending a pre-prepared dispersion of polyol (ethylene oxide capped polyether triol), Surfactant (Tegostab® B8870), catalyst (triethylenediamine in dipropylene glycol) with diphenylmethane diisocyanate (MDI) at room temperature. The blend was poured into a mold, allowed to cure and cut into rectangular cubes weighing 1.3 g. Prior to coating of the PU foams, LN and NFLN biocarbons were grinded using a Classic Line Fritsch Pulverisette 7 ball mill, and further grinded down with a pestle and mortar. 200 mg of the grinded biocarbons were dispersed into 100 mL of acetone using a Fisherbrand™ CPX2800 bath sonicator for 45 minutes. As shown in Fig. 8, to coat the surface to produce LN-PU and NFLN-PUs, the PU cubes were subsequently submerged in the acetone-biocarbon dispersions and shaken for 20 minutes. After coating, the LN-PU and NFLN-PUs were dried, prior to a final rinse with water to remove residual loose biocarbons. The coated PU cubes were finally dried once more overnight in an oven at 80 °C.

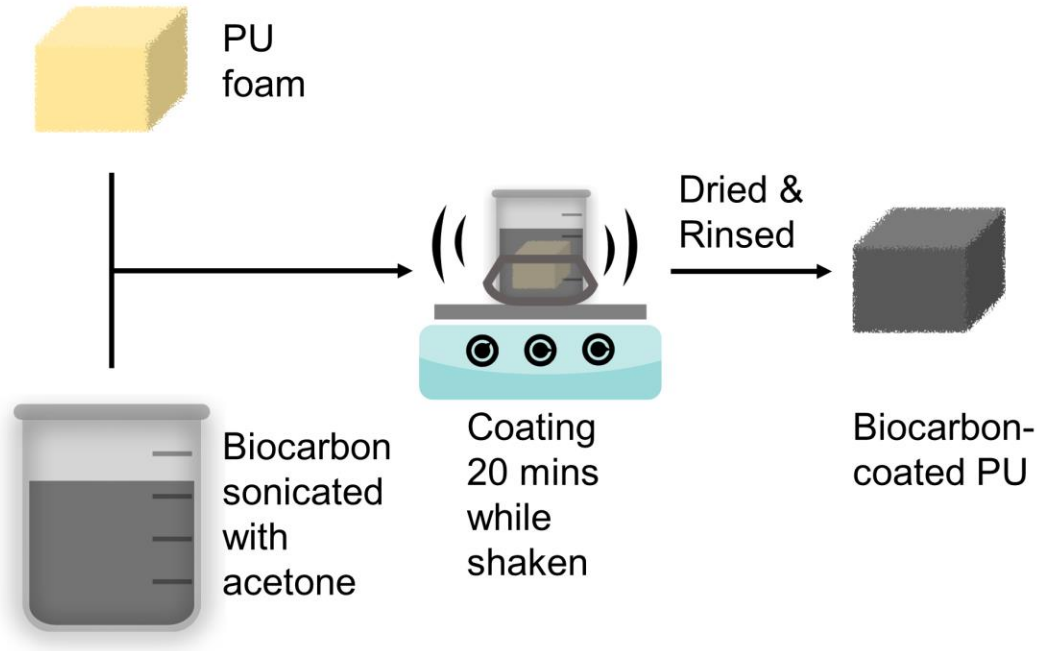

Fig. 8. Coating of the PU foams with LN and NFLN biocarbons.

3.6 Dye adsorption of methylene blue

The amount of biocarbon coated onto the PU samples was determined via TGA analysis. For each run, samples of 5 - 7 mg of PU were heated to 100 °C and held for 5 minutes, followed by heating to 800 °C at 20 °C/min in nitrogen gas. The amount of biocarbon coated on the PU was then estimated by the difference in the residue produced from the control PU and the total residue of the LN and FDLN-PUs as shown in Equation (1):

$$Biocarbon\ content\ (\%) = Total\ residue\ (\%) - PU\ residue\ (\%) \qquad \text{Eq. (1)}$$

For dye adsorption tests, 30 mL of methylene blue with concentrations of 5 and 10 mg/L were used for each coated-PU cube. A Cary 100 Bio UV-vis spectrophotometer was then employed to carry out absorbance measurements of the dye in the wavelength range of 380 – 780 nm. The adsorption of methylene blue was quantified by observing the decrease in the characteristic absorbance peak at 664 nm in the UV-vis spectra, which was then correlated to the concentration

of MB using a calibration curve. UV-vis measurements were taken at intervals of 30 minutes for a total duration of 150 minutes. The percentage removal of MB was calculated using Equation (2):

$$Percent\ removal\ of\ MB = \left[1 - \frac{C(t)}{C(0)}\right] \times 100 \qquad \text{Eq. (2)}$$

Where C(t) is the concentration of MB at time t, and C(0) is the initial concentration of MB.

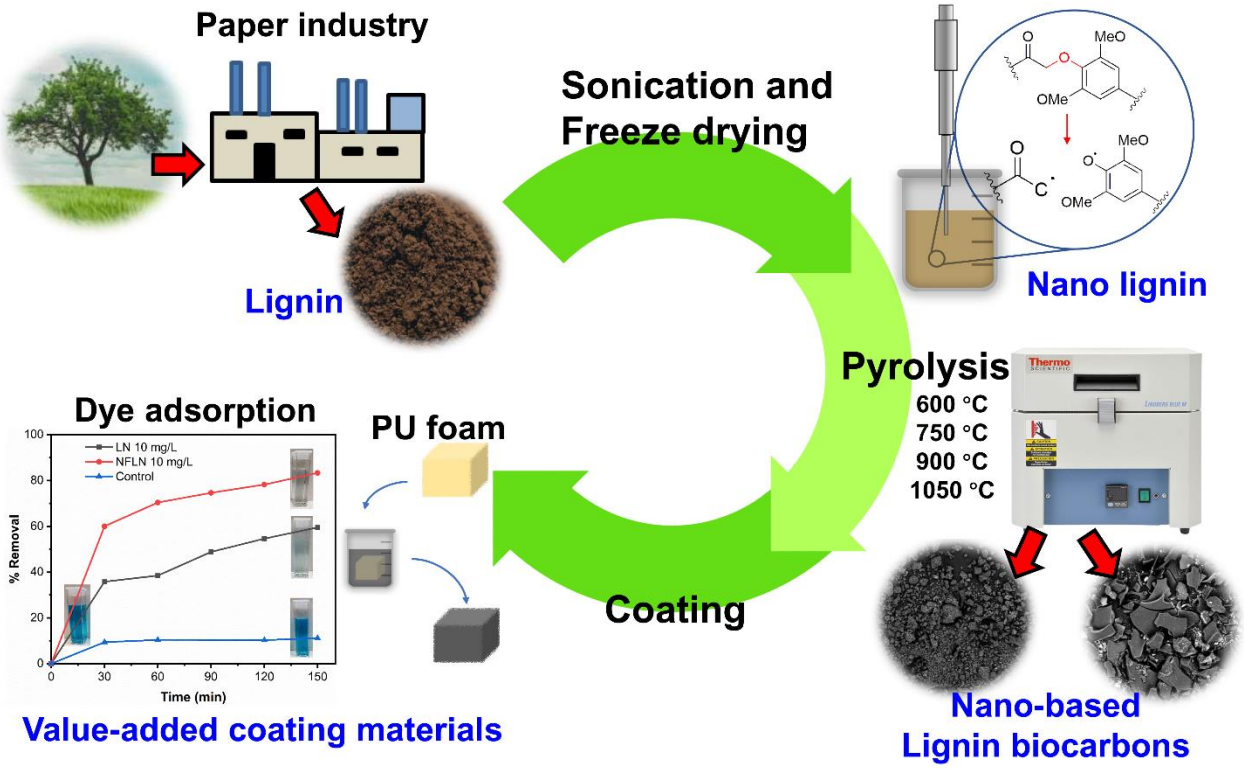

Fig. 9. Overall scheme for this work. Lignin having undergone treatment, carbonization and then used in application studies.

Chapter 4 Results and discussion

4.1 Particle size analysis and stability in water

4.1.1 Lignin nanoparticle fabrication

The LNs used are readily dispersible in water due to their sulfonic acid groups, with the extent of dispersibility dependent on the particle size and molecular weight. As seen in Fig. 10, after the sonication and freeze-drying treatment, NFLNs were able to disperse well in water whereas the untreated lignosulfonate demonstrated sedimentation, and required further mixing, such as via bath sonication, to obtain adequate dispersibility.

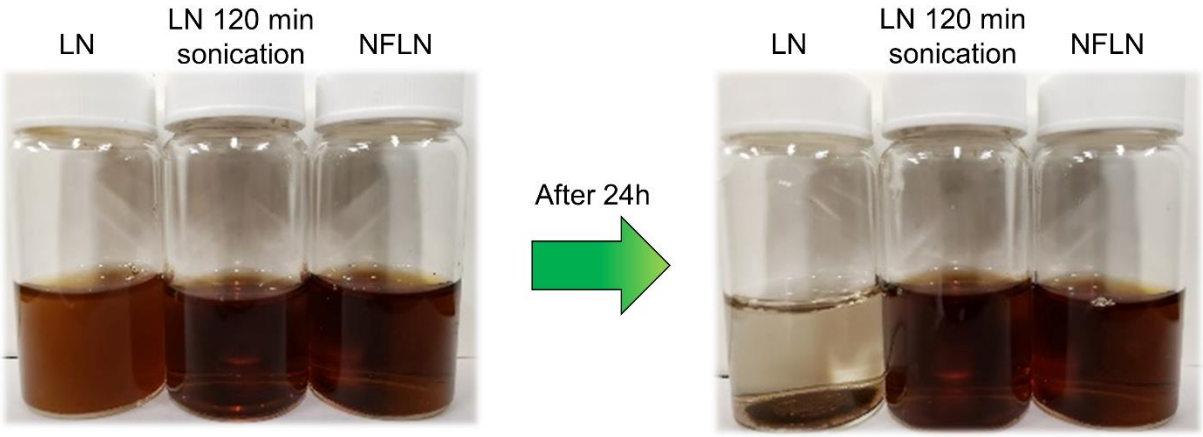

Fig. 10. Dispersion behaviour of LN and NFLN in water prior to and after sonication.

It has been suggested that lignin bonds such as the β-O-4 linkage, the weakest among the lignin ether linkages, can be cleaved by sonication, resulting in the gradual depolymerization of the lignin, and causing a simultaneous decrease in particle size and weight-average molecular weight [47,55]. As shown in Fig. 11a, a particle size reduction can be observed after an initial 30 minutes of sonication, compared to the initially large particle size of the untreated LN. As there was a slight decrease in the particle size with the employment of 2 h sonication versus 1 h, a 2 h sonication time was applied for all subsequent samples. As the dispersed LNs were polydisperse,

bimodal size distributions were used to characterize the samples as opposed to single average particle sizes. As the Zetasizer's light scattering technique was highly sensitive to the large particle sizes and dispersibility of the pristine lignin samples, a significant amount of variation was incurred. Despite this variability, it was evident that the initial particle size was well above an average of 0.5 – 1 microns, as observed from the consistently large peak averages.

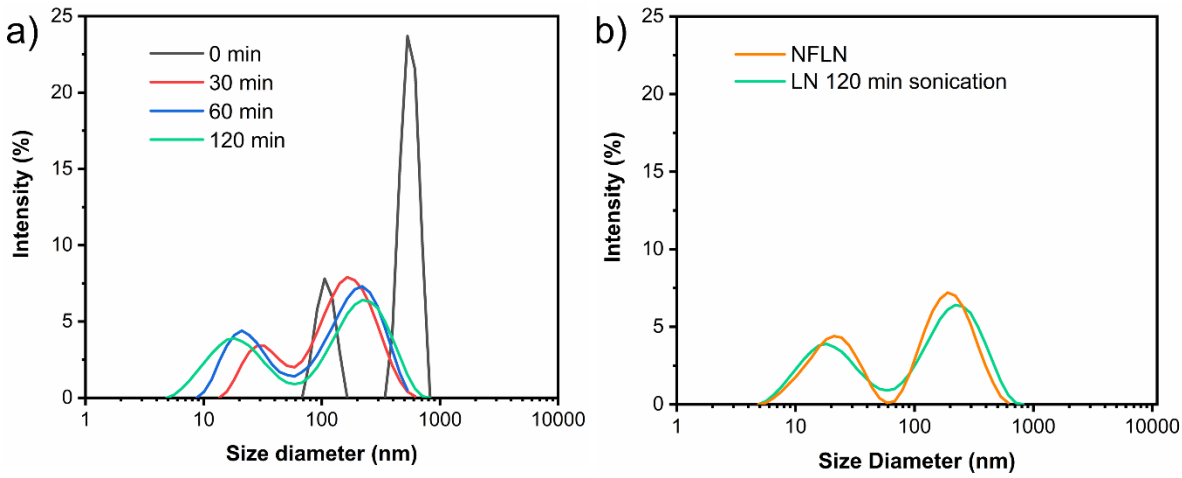

Fig. 11. (a) Particle size reduction at 30 mins to 2h, and (b) particle size comparison between untreated and redispersed NFLNs,

After sonication, the contribution of particle sizes to intensity has shifted down to bimodal peaks at approximately 20 and 220 nm. The presence of multiple peaks can be attributed to the breakdown of large lignin particles which were initially present and the inhomogeneity of the initial particle size distribution. Lignosulfonate dispersion after sonication demonstrated colloidal stability for over 6 months with no signs of sedimentation or re-agglomeration into larger particles. The lignin dispersions were then freeze dried to produce NFLNs as a precursor material for pyrolysis biocarbons, similar to a previously reported method for pyrolysis material preparation [100]. Although the dried NFLNs were observed to be micron-sized in its dried state, it is

demonstrated that the freeze-drying process only resulted in the agglomeration of the nano-lignins, as further redispersal into water results in the same size measurements obtained directly after sonication as shown in Fig. 11b.

Using the Zetasizer's static light scattering function to construct a Debye plot, the weight-average molecular weights of the untreated lignosulfonate and NFLN dissolved in DMSO were measured (Fig. 12). As a stable solution was necessary for the measurement purposes, DMSO was selected as the preferred solvent as it dissolves lignosulfonates readily, and the lignin used in this work demonstrated better solubility in DMSO in comparison to other solvents such as water. The static light scattering technique indicated that there was a reduction in the weight-average molecular weight of the lignin during the production of NFLNs, likely induced by the sonication process, which is also in line with the observations in other works[47]. Furthermore, the second virial coefficients obtained from the Debye plots were zero, indicating that DMSO was a theta solvent for the lignosulfonate, and would allow for the minimization of potential chain extension that could cause an inflated molecular weight measurements[112]

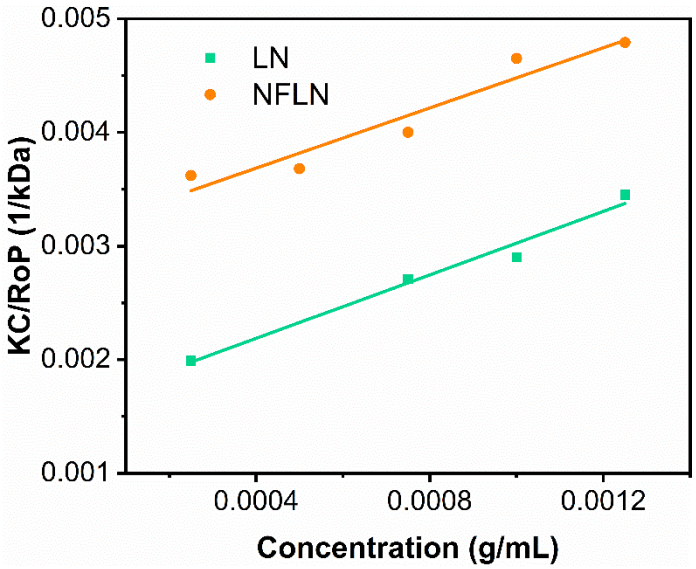

Fig. 12. Debye plot for weight-average molecular weight determination

4.1.2 Structural and thermal characterization of lignins and their respective biocarbons

FTIR analysis of the lignosulfonate display the typical characteristic lignin bands, with OH, methoxyl, and carbonyl functional groups present at 3425 cm^{-1}, 2840 cm^{-1} and 1760 – 1660 cm^{-1}, respectively as shown in Fig. 13[113,114]. A great number of other bands have been assigned to the lower wavenumber regions, including aromatic ring vibrations at 1595, 1513 and 1463 cm^{-1}, and C-O stretching from methoxyl groups at 1035 cm^{-1} [16,113]. Aliphatic CH stretching from methyl, methylene and methyne groups can be found between 3000 – 2860 cm^{-1} [113,114]. After pyrolysis, a reduction in functional groups and corresponding decrease in oxygenation is clearly observed by the smoothening of the spectra. The FTIR spectra of the LN and NFLN are similar, indicating that there was no significant difference in functionality between them.

Through pyrolysis, many of the functional groups are lost, including the hydroxyl and methoxyl groups from dehydration reactions[115] and the breakage of lignin linkages, starting with the weaker β-O-4 ether linkages and eventually with the ether 4-O-5 and phenyl 5-5 linkages, resulting in the evolution of oxygenated volatiles[10,116]. Furthermore, at temperatures approaching 600 °C, demethylation occurred, accompanied by the evolution of methane[117]. Between temperatures of 500 to 800 °C, the loss of the remaining lignin ether 4-O-5 linkages and other oxygenated groups occurred[10]. Overall, the FTIR spectra of the lignin derived biocarbons flattened with increasing pyrolysis temperature due to the loss in functionality and gradual conversion into a polycyclic aromatic biocarbon structure. However, the presence of minor IR peaks in the vicinity of 3425 cm^{-1} indicate of the presence of residual oxygen functionality on the produced chars.

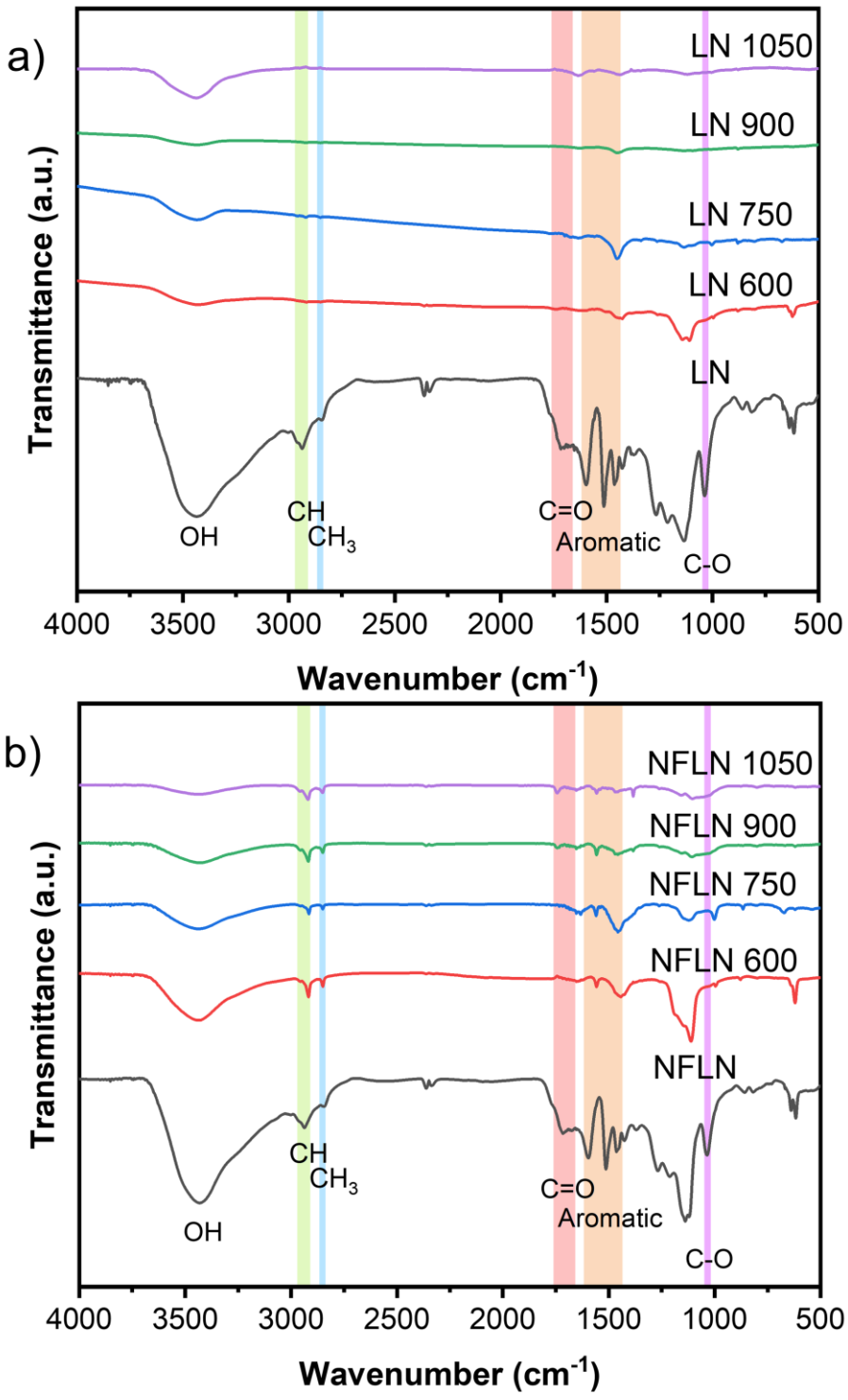

Fig 13. FTIR spectra of (a) LN and (b) NFLN, and after pyrolysis at various temperatures (600-1050 °C).

This loss in functional groups was further reflected in the TGA conducted under nitrogen to mimic pyrolysis in the tube furnace as shown in Fig. 14a. The mass loss approached a plateau at temperatures above 800 °C indicating the completion of the charring process. Further increase in temperature (up to 1050 °C) did not cause visible mass change in the TGA residues validating that most of the volatiles have already evolved. A comparison between the LN and NFLN find no significant difference in the thermal degradation behavior. Further comparison with the biocarbon yields obtained through pyrolysis in the tube furnace also corroborate this observation as presented in Fig. 14b. Variations in the biocarbon yield can occur as the pyrolysis rates are highly dependent on factors, such as temperature, heating rate, particle size, and residence time[10,118]. Variations in the yield obtained from the TGA curve at the respective temperatures are likely a result of differences in the equipment between the TGA and tube furnace. Despite this minor variation, the yields display the same downward trend.

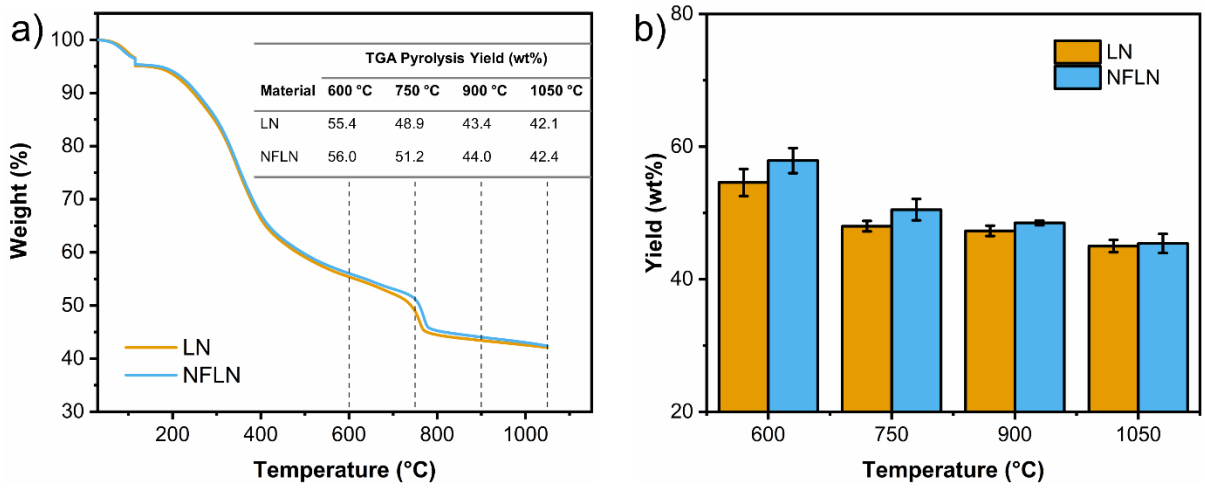

Fig. 14. (a) TGA curve of LN and NFLN and (b) their percentage yield from pyrolysis in the tube furnace

4.2 Morphological characterization

SEM was used to compare the morphology of the precursor lignins with respect to their carbonized biocarbons. The SEM micrographs of the LN and NFLN presented in Fig. 15 indicate their particle size ranged from small nanosized particles to large structures on the magnitude of several hundred microns. NFLNs that underwent freeze drying were found to rearrange into a number of platelet-shaped agglomerates. After undergoing pyrolysis, the overall structure of the biocarbons were found to resemble their precursor uncarbonized lignins. This is within expectations and prior studies have also reported the retention of original biomass structures or the dependence on the structure of the starting biomass after the pyrolysis treatment[74,75]. Furthermore, with increasing temperature, the elimination of structural impurities resulting in the smoothening of the biocarbon surface can be observed, formerly present in the lower carbonization temperatures.

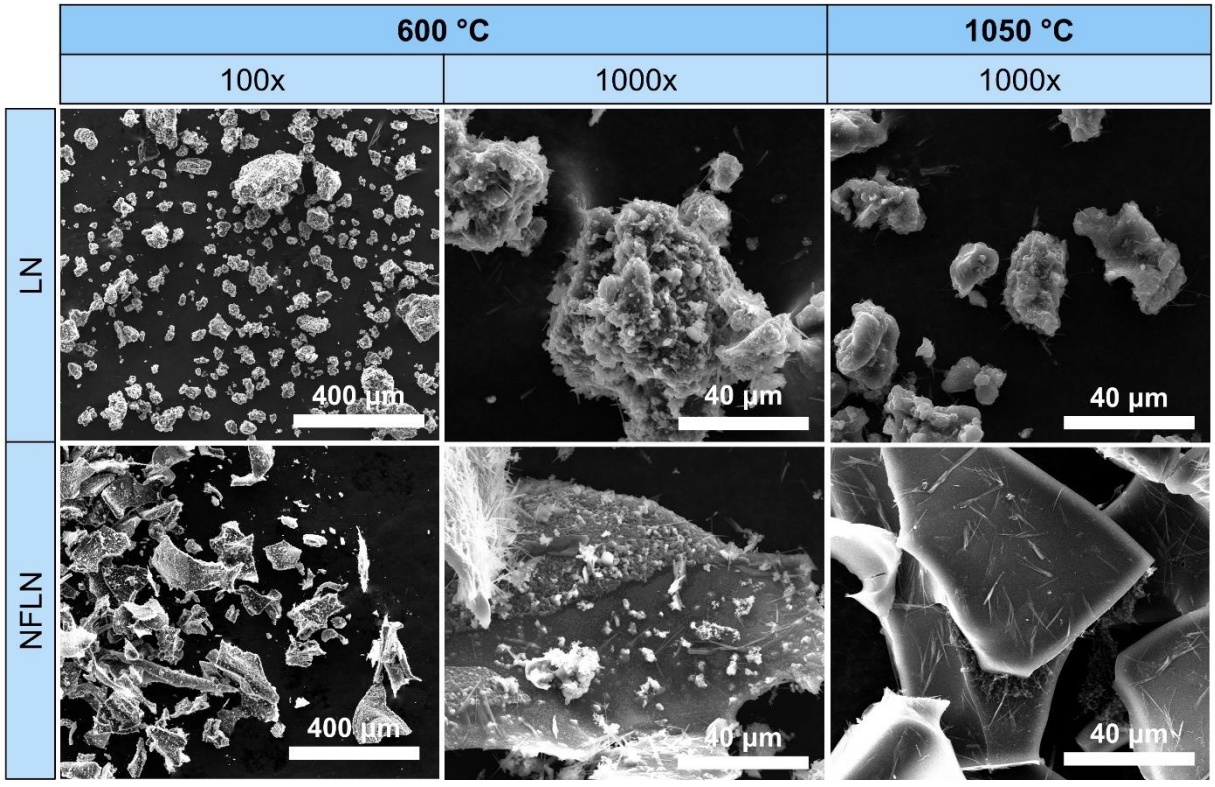

Fig. 15. FE-SEM images of LN and NFLN biocarbons at 600 °C, and 1050 °C.

Further sonication of the carbonized platelets proved that the platelets were no longer agglomerates, as no breakdown of the carbonized platelets into nanoparticles was observed. Under carbonization temperatures, the lignin can soften and then subsequently fuse to produce larger particles[119,120]. Furthermore, secondary recombination reactions, whereby volatile compounds can recombine into higher molecular weight products can occur. Volatiles repolymerizing onto the surface or pores of the biocarbons can produce secondary char[10,103].

4.3 Properties of LN and NFLN biocarbons

4.3.1 Elemental analysis and EDX mapping

The elemental composition of the samples was determined via elemental analysis, and EDX mapping was performed in order to observe the change in the elemental distribution with increasing carbonization temperatures. Increasing temperatures resulted in an increase in carbon content, followed by a reduction in sulfur and oxygen as confirmed by elemental analysis (Table 4). This was expected as volatiles are evolved out from the lignin with increasing temperature. An EDX spectrum conducted on the needle structures found them to be considerably more oxygenated than the surrounding overall biocarbon composition but was still composed of a distribution of the four elements. The presence of a visible amount of sodium in both elemental analysis and EDX mapping can be attributed to its presence in the initial lignosulfonate material emanating from the extraction process. The yields observed in the carbonization experiments are in agreement with various other works performed on lignin pyrolysis around this temperature range, which have been reported to range from approximately 40 to 52%[100,113]. In comparison to cellulose and hemicellulose, the yield of biocarbon for lignin is relatively higher due to its greater thermal stability[118]. The thermal stability of lignin is associated with the high aromatic benzene ring content that is already present in the lignin. The carbonization of the lignin involves the conversion of the

structure into benzene rings, which then combine to form the aromatic polycyclic structure of char[10].

Table 4. Summary of elemental composition, biocarbon pyrolysis yield, and BET surface areas

Material	Pyrolysis Temperature (°C)	Elemental Composition*			BET Surface Area (m^2/g)
		C (%)	S (%)	O (%)	
LN		52.5	4.9	34.4 (2.50)	**
	600	71.1 (1.23)	3.4 (0.45)	16.9 (0.06)	0.92
	750	72.1 (1.67)	4.0 (0.06)	14.7 (0.78)	1.69
	900	84.0 (0.79)	2.3 (0.04)	8.9 (0.23)	1.95
	1050	87.3 (0.86)	1.0 (0.18)	6.3 (0.54)	8.00
NFLN		49.5	4.3	33.0	0.71
	600	68.0 (0.05)	2.6 (0.91)	17.7 (0.99)	0.94
	750	74.6 (0.6)	3.5 (0.09)	15.7 (0.03)	10.23
	900	82.2 (0.58)	2.2 (0.63)	10.3 (0.84)	12.76
	1050	87.1 (0.87)	1.1 (0.38)	6.7 (0.40)	72.47

* Values are average of three measurement (standard deviation)

** Instrument unable to measure surface area

The surface of the biocarbons reflected the change in elemental composition as shown by the EDS mapping in Fig. 16. Initially, both LN and NFLN have similar intensities, indicating the presence and distribution of carbon, oxygen, sulfur and sodium elements throughout the surface. With increasing pyrolysis temperatures, the intensity of the carbon increases significantly relative to the intensities of the other elements, due to the significant shift in elemental composition to a

high-carbon content char. The relative intensity of the oxygen, although still present at lower pyrolysis temperatures, significantly decreased due to the evolution of volatiles and loss in oxygenated functional groups as seen in the FTIR. Sulfur, which is characteristically found within the sulfonic groups of lignosulfonates evolved into sulfur dioxide during the pyrolysis[121].

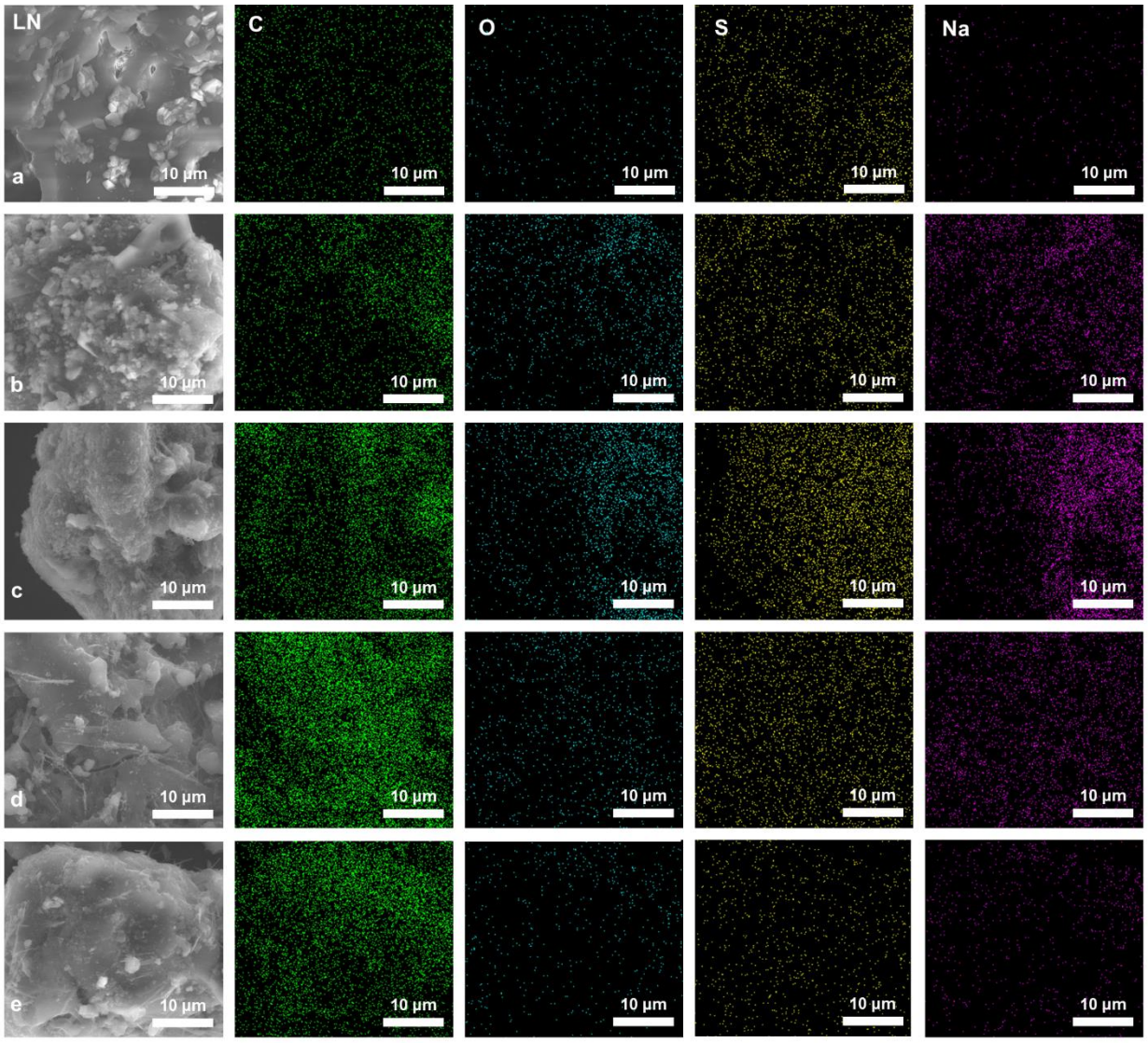

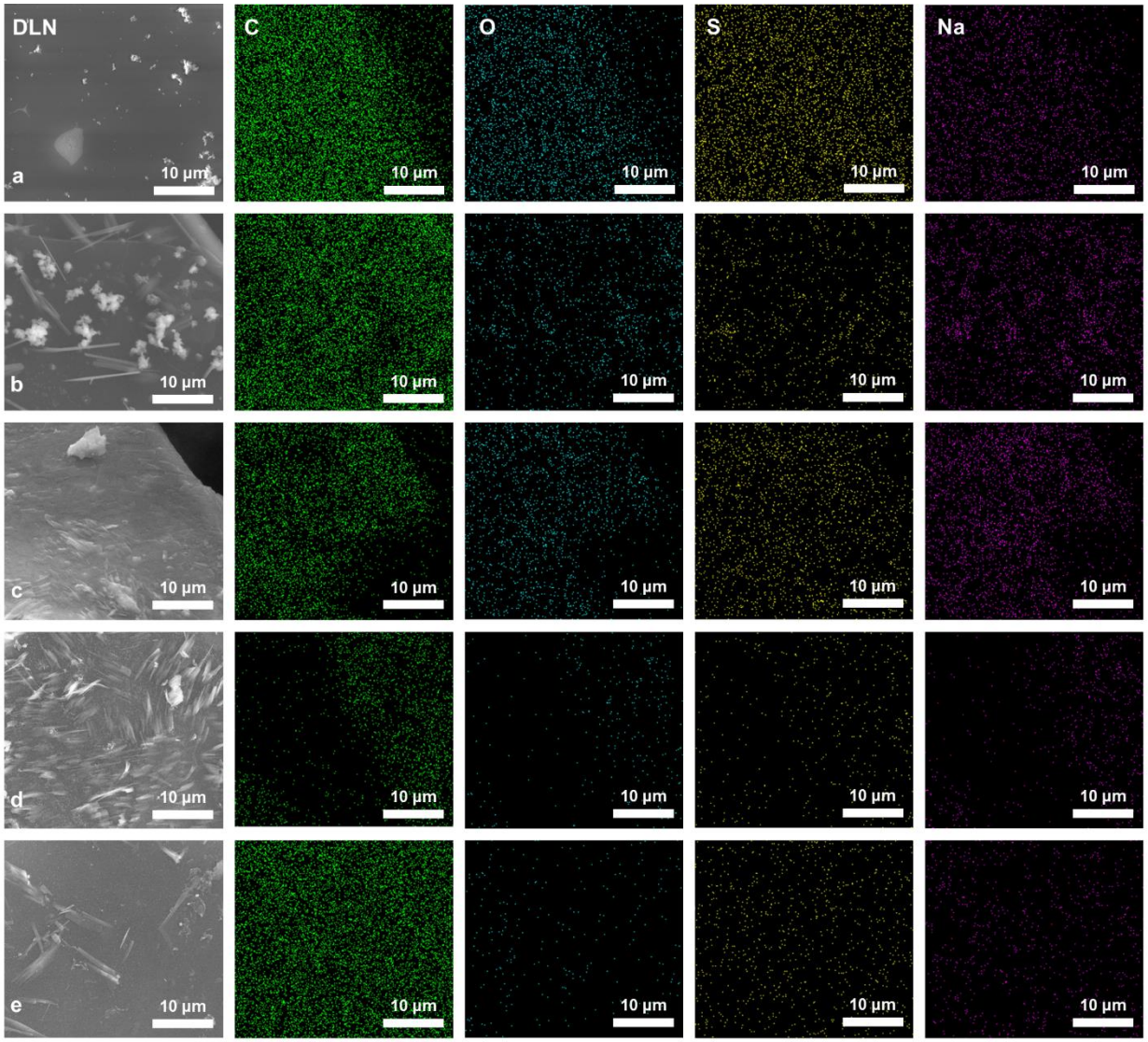

Fig. 16. EDS Mapping of lignosulfonate (Top) and NFLN (bottom) biocarbons: (a) LN/NFLN, (b-e) 600 – 1050 °C

4.3.2 BET Surface Area

The development of porosity in biocarbons is dependent on the precursor material[122] and can be further increased by either physical or chemical activation depending on the selection of the activator materials[123]. The BET surface areas as displayed in Table 4 demonstrate an increasing trend with increasing pyrolysis temperatures. This is in agreement with well-established knowledge on the opening of pores on biocarbons at high temperatures, which are necessary to

draw out the volatile materials to leave behind a porous structure. The BET surface areas for the LN biocarbons can be observed to be significantly lower, as porosity was also not evident in the lignosulfonate in the SEM imaged. Freeze drying has been performed in various studies to impart a porous structure onto the dried lignin, both through the use of solely freeze drying[99] or in combination with an additive[100]. By adjusting the concentration of the lignin in water, the morphology of the freeze-dried lignin can be modified resulting in changes in sheet-like particle thickness, or even changes to different shapes and structures[99]. These structures can be further stabilized using either low temperature annealing or high temperature carbonization. As a result, various freeze-dried lignins can be produced as precursors to porous carbons, ranging from structures with zero surface area[100], to structures with as high as 702 m^2/g[99]. In this work, the produced NFLNs exhibit surface areas on the lower end, as they were optimized for weight yield rather than surface area; however, they still have displayed noticeably higher surface areas than the LN biocarbons.

4.4 XRD

Fig. 17 presents the XRD spectra of the LN and NFLN precursors and biocarbons pyrolyzed at different temperatures. Visible throughout the biocarbon spectra are broad peaks at 2θ values of around 23.5° and 43.5°, corresponding to the turbostratic carbon crystallites on the planes 002 and 100, respectively[124]. These broad peaks are characteristic of amorphous carbons, representing a degree of short-ranged order. A slight increase in peak intensities can be observed with increasing pyrolysis temperatures, indicating a gradual transition towards a more ordered graphitic structure[125,126]. Additional sharper peaks can be noted in the spectra at lower pyrolysis temperatures below 1050°C, indicative of the presence of inorganic compounds in the initial LN, attributed to NaCl, Na_2SO_4 and Na_2CO_3[127–129]. The loss of these impurities at higher pyrolysis

temperatures was corroborated by the elemental analysis result, as seen by the reduction in sulfur composition, as sodium sulfates can react with the carbon structure to produce sodium sulfides[127]. The spectral features of the biocarbons greatly resemble that of other reported biocarbons[124,125]. Overall, no significant difference in elemental composition and in the XRD spectra were observed between either of the lignin and NFLNs, including between their respective carbonized states.

The previously seen increase in surface area can also be attributed to the presence of inorganic impurities such as sodium carbonates as seen in the XRD spectra, which have been suggested to increase porosity in the carbon structure through an alkaline carbonate activation process[127,130]. In the activation process, the alkaline carbonates are thermally decomposed, resulting in the evolution of CO_2 and formation of surface salt sites[131], which correspond to the reduction and eventual complete disappearance of peaks on the XRD spectra.

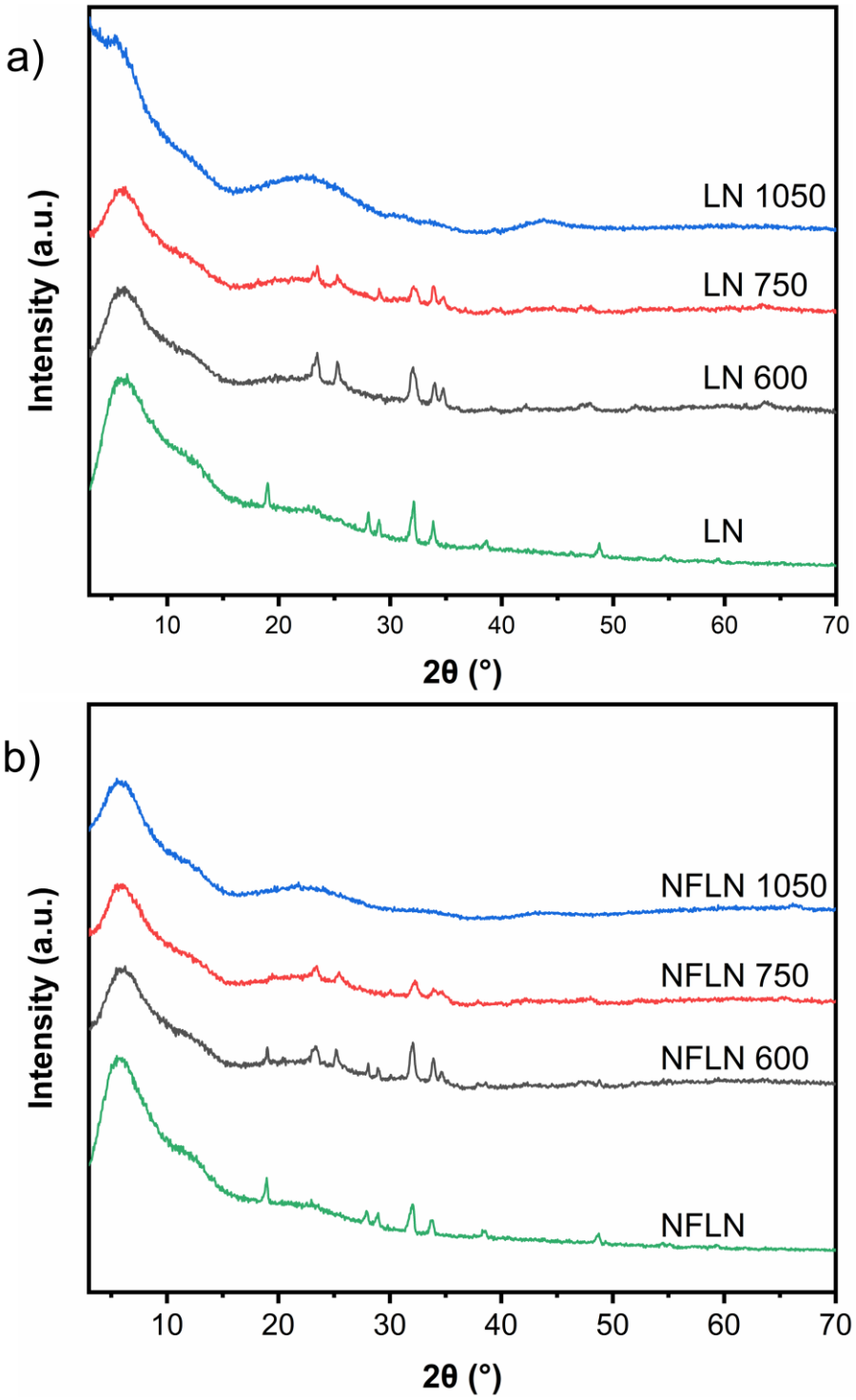

Fig. 17. XRD spectra of (a) LN and (b) NFLN, along with their respective biocarbons.

4.5 Raman spectroscopy

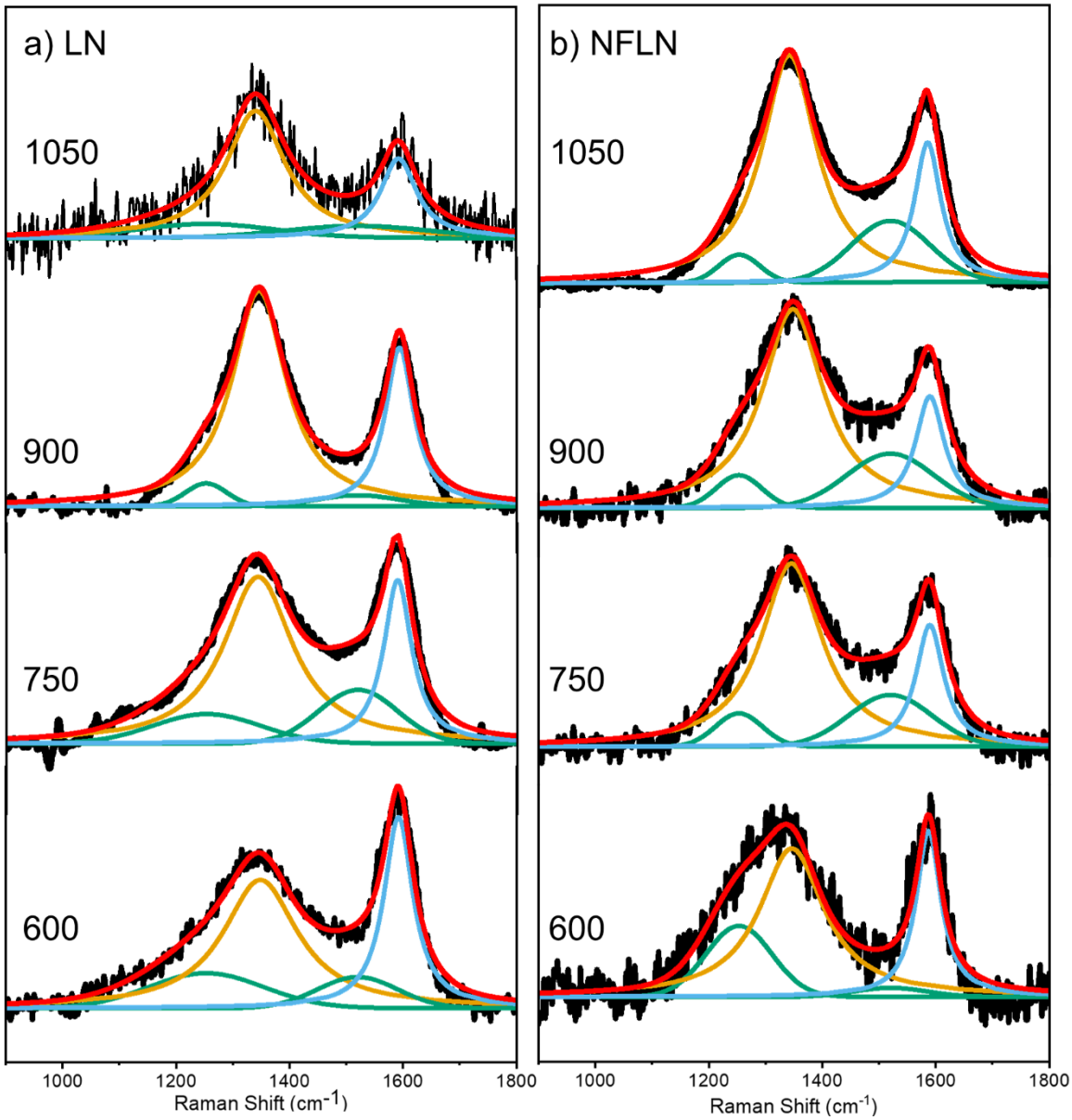

Fig. 18. Raman spectra of (a) LN and (b) NFLN biocarbons at 600 – 1050 °C pyrolysis temperatures.

The Raman spectra of the carbonized lignins as shown in Fig. 18 display the typical features of amorphous carbon materials. The deconvolution of Raman spectra using from as few as two to as many as ten bands has been reported in literature, attributing the various bands to structures

present in the chars to obtain more precise fittings[104,126,132,133]. The D and G bands produced from sp^2 bonded carbon atoms, specifically attributed to disordered turbostratic carbons near 1350 cm^{-1} and highly-ordered graphitic carbons near 1580 cm^{-1}, respectively, are the major bands of note when performing the characterization of carbonaceous materials[104,134–136]. For both LN and NFLN biocarbons, four bands were assigned to obtain a good fit as per the work of Ribeiro-Soares et al.[137], using Lorentzian bands for the D and G, along with the addition of two Gaussian bands associated with highly-disordered areas, which were fixed at 1253 and 1520 cm^{-1}. The Tuinstra-Koenig relation involving the ratio of the intensity of the D to G peak in carbonaceous materials, or I_D/I_G ratio, is well known and has been used extensively to characterize the content of graphite-like structures[135,138]. The gradual increase in I_D/I_G ratios, as seen in Fig. 19, with increasing temperatures is in line with the observations of other works involving the carbonization of biomass around this temperature range[12,139,140]. This increase has been ascribed to the aromatization of the biomass structure, through the condensation of smaller aromatic rings into larger aromatic structures as a result of high temperature treatment[138,141]. Overall, a higher I_D/I_G ratio can be seen for the NFLN biocarbons, indicating a higher ratio of aromatic ring structures with defects comparable to the ordered graphene structures in LN biocarbons. As this trend is present throughout the pyrolysis temperatures, it is likely that the treatment for the conversion of LN to NFLN via sonication and freeze-drying contributed to this increase in disordered structure.

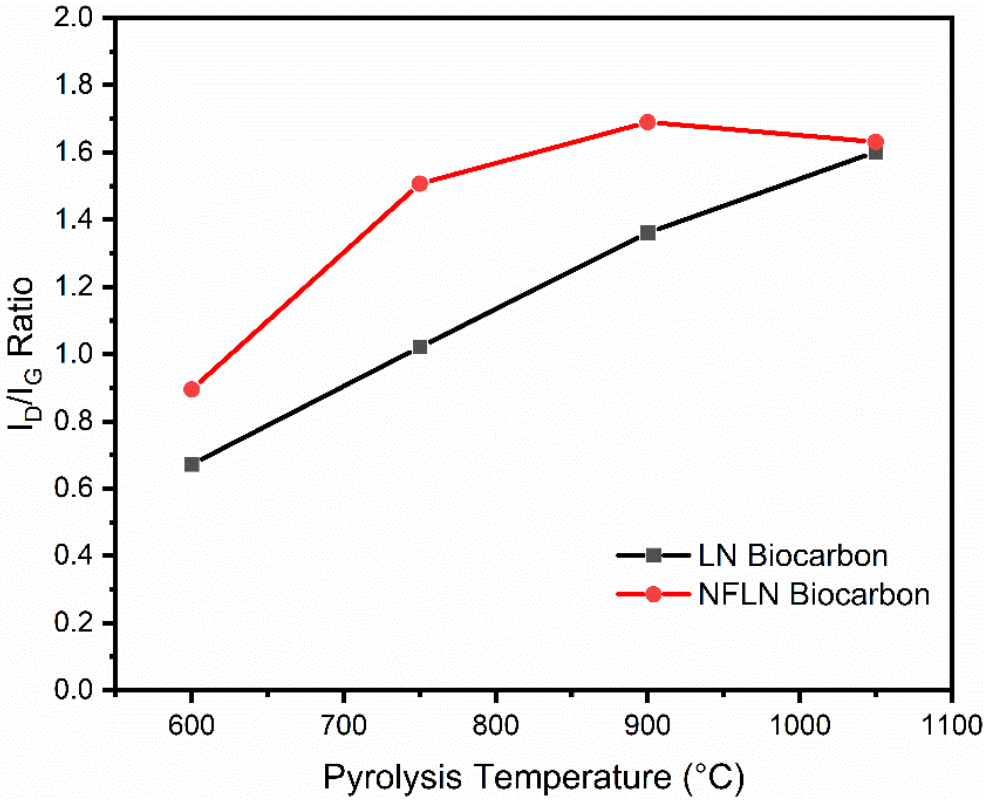

Fig. 19. Change in I_D/I_G with increasing pyrolysis temperature for both LN and NFLN biocarbons.

4.6 Methylene blue adsorption using biocarbon-coated polyurethane foam

Both LN and NFLN biocarbons were first grinded down and then dispersed into acetone to coat polyurethane (PU) foams. The NFLN biocarbon dispersed more effectively in the acetone and hence coated more effectively onto the surface of the PU, as seen in Fig. 20 at both concentration of 5 mg/L and 10 mg/L, which is further corroborated by the darker color of the NFLN-PU.

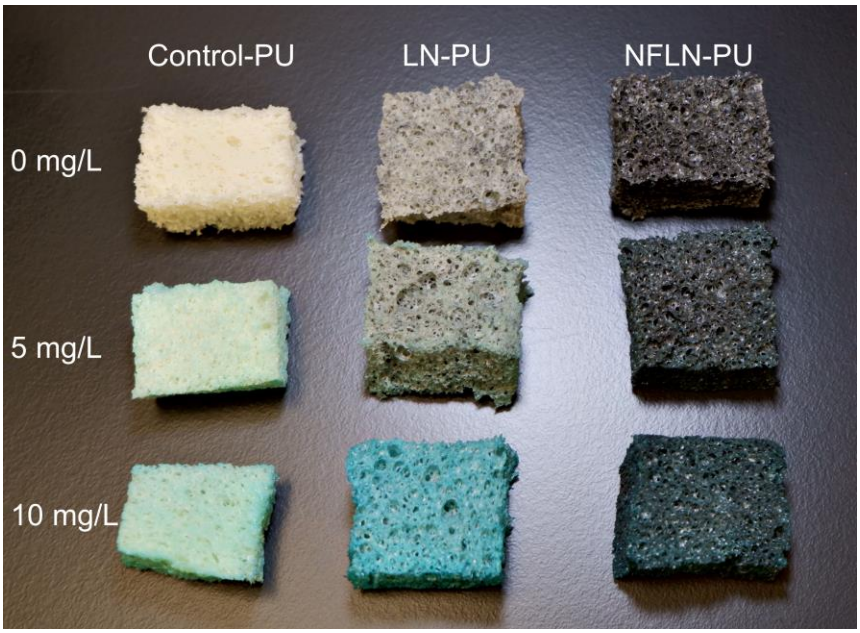

Fig. 20. PU foams before and after dye adsorption tests

The amount of biocarbon coated is shown in Fig. 21a determined via TGA analysis using Equation 1 (Fig. 22b) from the weights of the decomposed residues. The amount coated constituted 3.0 ± 0.4 and 4.3 ± 0.5 wt.% of the LN and NFLN-PU's respectively. The zeta potentials of the LN and NFLN biocarbons were measured to be -36.5 ± 1.9 and -44.9 ± 1.5 mV (Fig. 9b), respectively. Negative surface charges in the case of other carbonaceous materials, has been attributed to the presence of acidic functional groups and is further confirmed by elemental oxygen composition[142]. The observed zeta potential difference between LN and NFLN could be attributed to the grinding pre-treatment both materials underwent. A particle size analysis of 0.1 wt% of biocarbon dispersed into water found that the majority of the NFLN biocarbon was submicron in size, whereas a significant portion of the LN biocarbon was still in the micron size range. While both materials underwent the same treatment, preliminary results indicated that the NFLN was easier to grind than the LN biocarbon likely accrued from the sonication - nanomaterial production process and employed freeze-drying in the NFLN samples. Furthermore, as a direct consequence of improved grinding, it is likely that any new exposed surface would have been more oxidized

and thus may account for the discrepancy in zeta potential. Overall, larger micron-sized particles of the LN biocarbon were found to wash off during rinsing and thus were not conducive to achieving a higher coating content.

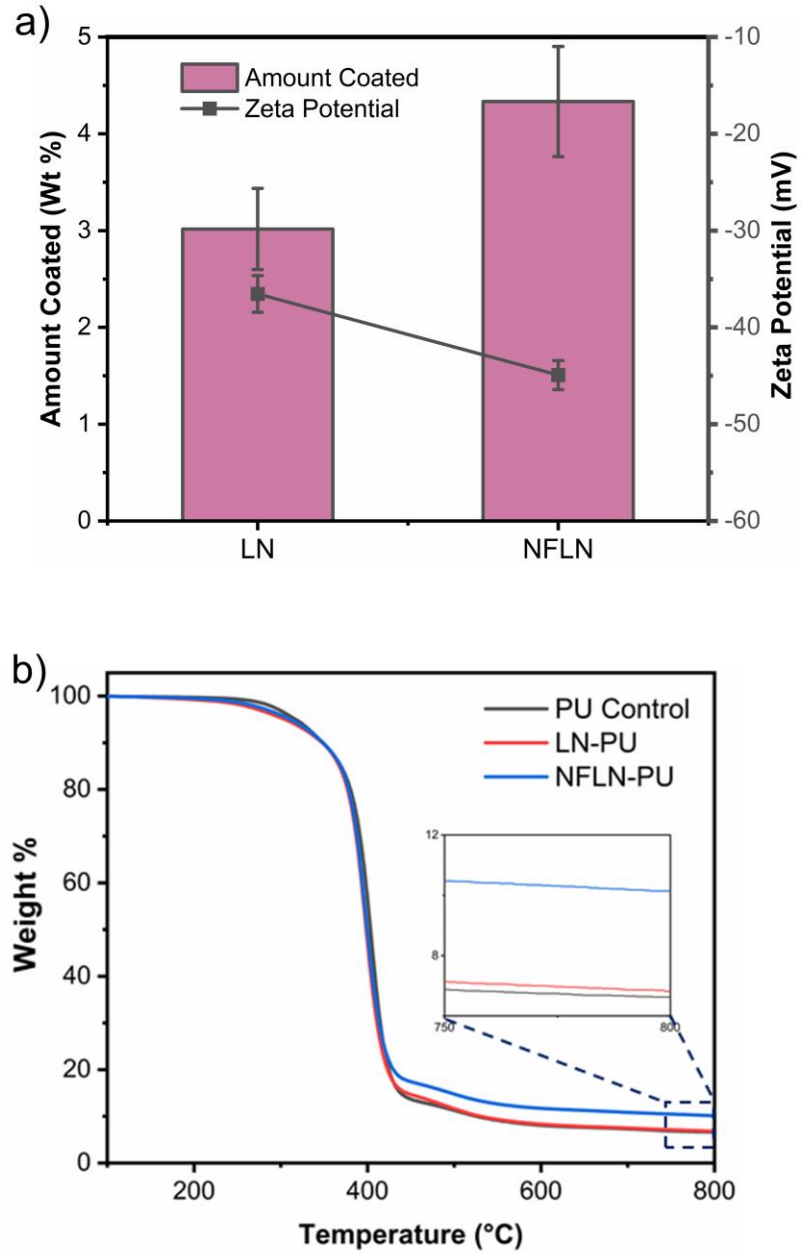

Fig. 22. (a) Amount of biocarbon coating and its zeta potential, and (b) TGA for determination of biocarbon amount.

Work into the optimization of MB dye adsorption using the coated LN and NFLN-PUs was performed by varying the concentration of dye from 1 mg/L to 10 mg/L, with the range selected based upon the works of other adsorbent coatings[83,84]. For example, in a study by Lefebvre et al.[83], carbon nanotubes were used for foam coating for concentrations of 6.38 mg/L of dye. A calibration curve was used to relate the concentration of MB to the absorbance values obtained from UV-vis curves (Fig. 23). This calibration curve was created by producing a range of known concentrations of MB relevant to the following dye adsorption studies.

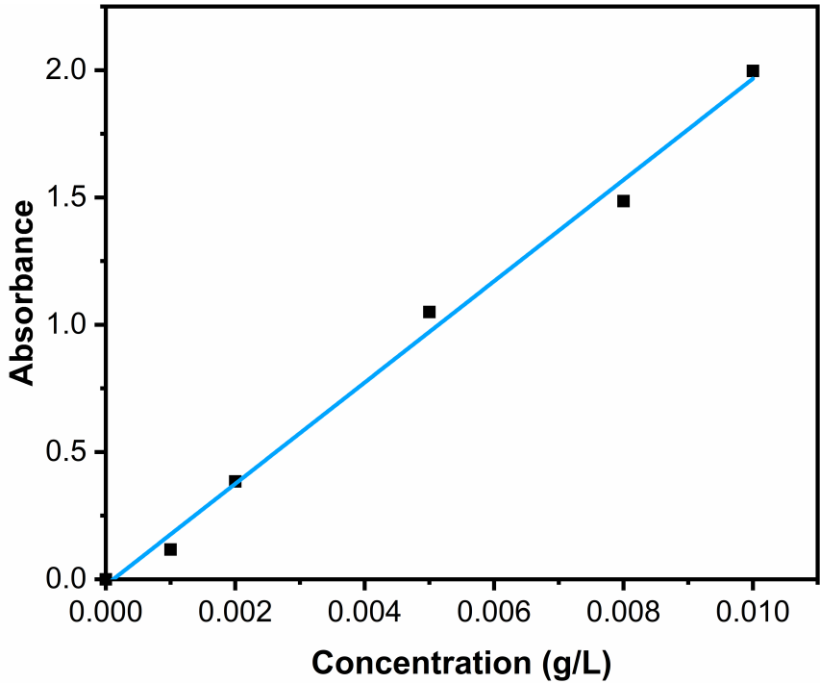

Fig. 23. Calibration curve used to correlate absorbance from UV-vis spectra to concentration of MB dye.

As preliminary studies showed that similar amounts of methylene blue were removed between 1 mg/L to 5 mg/L, dye concentrations of 5 mg/L and 10 mg/L were selected for a more comprehensive time study. The UV-vis curves are presented in Fig. 24, which show the gradual reduction in methylene blue dye over time, which were subsequently then converted into

percentage removal. As a result, it was shown that both LN and NFLN biocarbons demonstrated promising results for use as both an adsorbent, and coating for polyurethane foams.

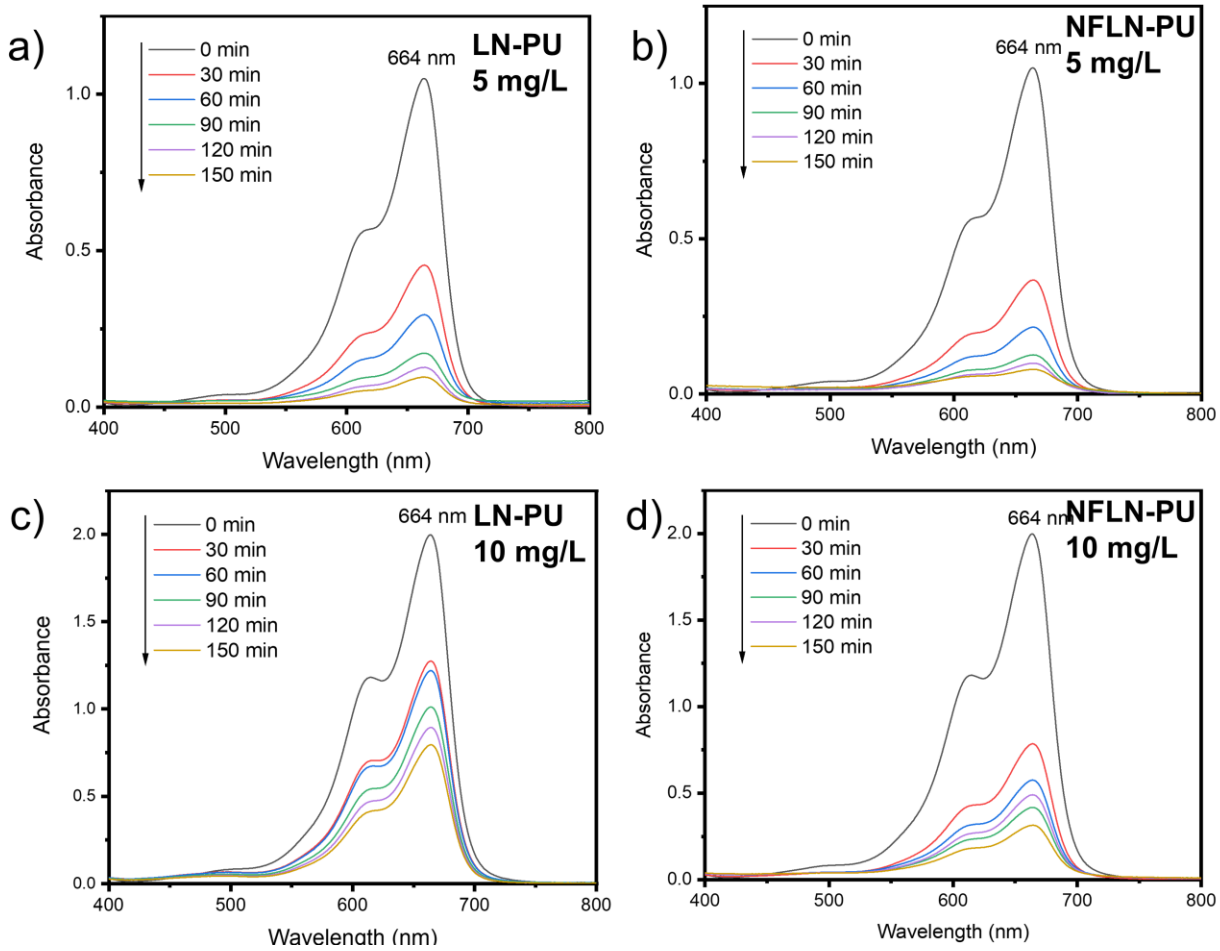

Fig. 24. UV-vis spectra demonstrating dye removal with respect to time for LN and NFLN-PUs at 5 mg/L (a, b) and 10 mg/L (c, d) respectively.

As shown in Fig. 25a and 25b, the uncoated polyurethane foams do not demonstrate significant adsorption of the dye, exhibiting an average 11% removal of MB at both concentrations. By coating the foams with LN and NFLN biocarbons, a significant increase in adsorption capacity is demonstrated with a 90% removal of dye at 5 mg/L. By doubling the dye concentration, the NFLN-PU outperformed the LN-PU with a removal efficiency of 83.3% and 59.5% respectively.

As indicated previously, the biocarbons which possess a negative surface charge facilitate dye adsorption of the positively charged cationic methylene blue dye due to electrostatic attraction between the opposing charges. The higher negative zeta potential of the NFLN biocarbon provides insight into the effectiveness of NFLN over the LN biocarbon in the adsorption of MB. Furthermore, the most important parameter for adsorbent materials is the surface area, which determines the availability of sites for adsorption. As a result, the higher surface area of the NFLN biocarbon likely plays a role in achieving better adsorption, in addition to contributing to the lower zeta potential. It can also be seen that the smaller particle size of the NFLN biocarbon enabled the coating of more adsorbent onto the foam and explains the major discrepancy between the performance of two biocarbons, as the adsorption capacities for both biocarbons translates to approximately 4.5 mg_{dye}/g_{carbon}. This adsorption capacity is relatively low in comparison to conventional adsorbents as no activation process was employed to develop higher surface area. For example, carbons which have undergone activation processes can have surface areas as high as 1000 m^2/g[143]. Overall, as indicated by the performance of both biocarbons, there is room for further optimization by extending the range of dye concentration, as well as optimizing the particle size and surface area to enhance PU coating and dye adsorption.

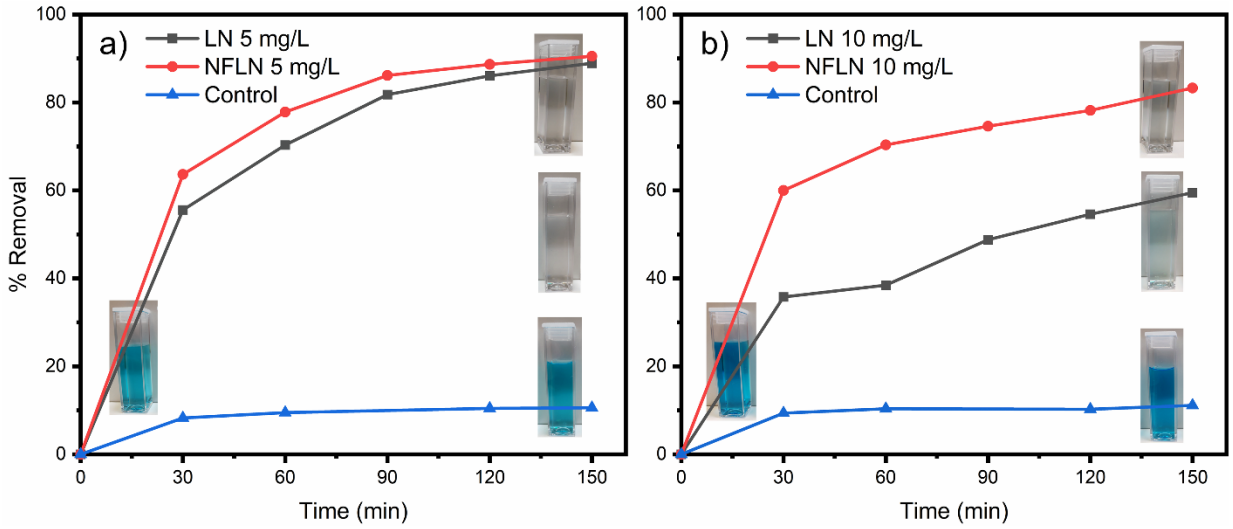

Fig. 25. Methylene blue dye adsorption of the biocarbon-coated PU foams at different concentrations: (a) Percentage removal of MB at 5 mg/L and (b) Percentage removal of MB at 10 mg/L.

4.7 Mechanical properties of natural rubber composites

For preliminary work investigating the use of lignin biocarbon in composites, LN biocarbon pyrolyzed at 900 °C was first grinded down and dispersed to water, prior to its addition into a natural rubber formulation at 5 and 10 phr. Both biocarbons were constantly stirred to avoid settling and were observed to adequately disperse in their formulations. Upon casting to produce natural rubber films with LN biocarbon as a filler, samples were cut out into specimens of around 50 mm in thickness and measured for mechanical properties. As seen in Fig. 26a and 26b, the tensile strength was seen to increase by 18.7% at 10 phr. The increase in tensile strength corresponds to an increase in the film's stiffness, as evidenced by the increase in modulus (Fig. 26c) where at 50% and 300% elongation, a 40% increase in modulus was observed. This increase in modulus is a result of the hardness and high moduli of the biocarbons. As seen in Fig. 26d, a 15% increase in tear strength was observed in both loadings. Despite a gradual increase in tensile

strength at progressively higher loadings of biocarbon, the tear strength of the natural rubber films were found to remain constant at both 5 and 10 phr of biocarbon. Overall, the reinforcing effects are in line with expectations, as various carbon fillers have been used as fillers successfully to improve mechanical properties in rubbers. In a study by Jiang et al.[13] where lignin was carbonized and used in styrene-butadiene rubber, and observed noticeable increase in mechanical properties at loadings of up to 40 phr.

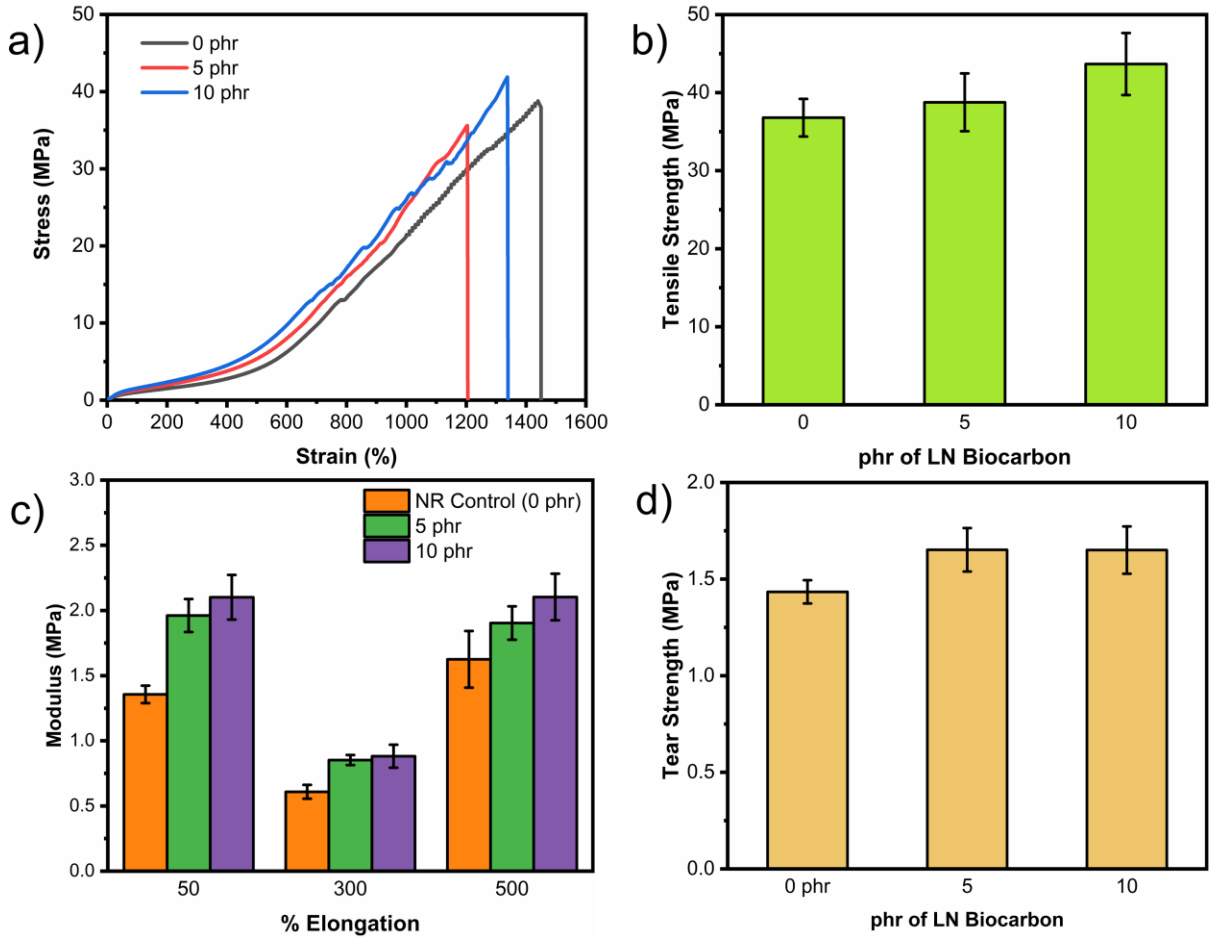

Fig. 26. (a) Tensile curves, (b) tensile strength, (c) modulus at 50%, 300% and 500% elongation, and (d) tear strength of NR films with LN biocarbon as a filler.

Additional work into investigating the use of NFLN, and further optimization of the carbon loading and filler properties such as particle size can be conducted. However, it should be noted

that as the LN chars were found to have residual oxygen present in the elemental composition of the chars, further improvements may be realized by the usage of other rubbers with some degree of polar functional groups, such as acrylonitrile rubber and chloroprene or functionalized rubbers. Selection of a compatible rubber is pertinent as has been demonstrated for more polar fillers such as cellulose nanocrystals, where rubbers such as chloroprene[88] and styrene-butadiene rubber[3] have been used. As an alternative, the LN or NFLN rubbers can be pyrolyzed to further deoxygenate the chars. By enhancing the compatibility between rubber and filler can facilitate further polymer-filler interactions to produce a greater reinforcing effect.

4.8 Conclusion

In this work, platelet-like lignin nanoparticles (NFLNs) were produced using probe sonication and freeze-drying that were further pyrolyzed into biocarbons and compared with pristine lignin (LN) based biocarbons. The LN and NFLN biocarbons, along with their precursors, were charactered both morphologically and functionally. Prior to pyrolysis, NFLNs were observed to be smaller in particle size and weight-average molecular weight as a result of the chain cleavage via the sonication treatment. Through FTIR, TGA, elemental analysis and XRD, it was confirmed that the sonication-freeze-drying treatment did not translate into any detectable chemical or functional difference in the biocarbons post pyrolysis. As a result, the treatment was determined to have left primarily a morphological change into the reorganization of lignin nanoparticles into micron-sized platelet-like particles as observed by SEM. These platelet-like particles retained their shape after undergoing carbonization and exhibited greater surface area. Higher carbonization temperatures of up to 1050 °C resulted in high carbon-content (87%) with a yield s of 45 wt%. Preliminary studies into the coating of PU foam for the adsorption of methylene blue found that the NFLN outperformed the LN, with a dye removal of 83.3% as compared to 59.5% for the LN.

Further preliminary tests into the addition of LN biocarbon into NR films demonstrated an increase in tear and tensile properties. Overall, a facile production of nano-based lignin biocarbon developed in this study demonstrated high adsorption efficiency towards cationic dyes, demonstrating its ability to be used as an additive for PU foam-based filter materials and potentially other applications, such as a pigment, coating or filler of polymer systems. Further steps can be taken to optimize the performance of LN and NFLN biocarbons in both coating and filler applications through more comprehensive tests.

Chapter 5 Concluding remarks and future work

As society continues to transition towards sustainable materials and processes, the use of renewable resources is becoming progressively important. As lignin is abundant in the biosphere, and thus is a renewable biopolymer, it is environmentally appealing to implement its use. Furthermore, as it has traditionally been limited to low-value applications, and has been largely untapped as a resource, there is much interest in its valorization from both an economic and environmental perspective. Lignin's high aromaticity and carbon content is conducive to obtaining higher yields of biocarbon through pyrolysis.

The work described in this thesis covers the valorization of lignin, an abundant biopolymer that has renewable origins and versatile properties as a precursor to carbonized materials for use as an adsorbent, coating, pigment and filler of polymer systems. In this work, lignin was pretreated through sonication into nanoparticles, whereby a reduction in particle size and weight-average molecular weight was observed. These nanoparticles were then freeze-dried to produce NFLN as a precursor for carbonization into biocarbon. LN and NFLN were then carbonized into biocarbon via pyrolysis at temperatures of 600, 750, 900 and 1050 °C. The properties of NFLN, and LN biocarbon produced from pristine lignin via pyrolysis were characterized and compared. Overall, both biocarbons were observed to have increasing carbon contents at higher pyrolysis temperatures, which was in line with expectations, with significant carbon contents of 82% and 87% at 900 °C and 1050 °C respectively. NFLNs were found to rearrange into platelet-like particles and exhibit different morphologies as seen through FE-SEM but were functionally determined to be similar as validated via FTIR, SEM, and XRD. Furthermore, NFLNs were found to have higher BET surface areas as a result of the sonication and freeze-drying treatment. With a significant carbon contents

and enhanced surface area, the NFLN biocarbon displayed promising properties for use as an adsorbent, and filler.

LN and NFLN biocarbons pyrolyzed at 900 °C were ground into sub-micron particles using ball milling and deposited on the surface of PU foam for the adsorption of methylene blue dye. Using TGA analysis to determine the amount of biocarbon successfully deposited onto the surface of the PU, it was found that the NFLN biocarbon coated more effectively. Adsorption studies of methylene blue at 5 mg/L found that both biocarbons removed similar amount of dye, but that the NFLN-PUs removed significantly more dye at 10 mg/L. This was further corroborated by the lower NFLN biocarbons zeta potentials, due to the electrostatic attraction between the dye and biocarbon.

LN biocarbons pyrolyzed at 900 °C were incorporated into NR film composites to provide mechanical property enhancement, and offer a sustainable reinforcement material alternative to petroleum-based carbon fillers such as carbon black. Preliminary tests using 5 and 10 phr of LN biocarbon showed an increase in tensile and tear properties.

Further work into the optimization of the dye adsorption properties of the biocarbons can be performed, to fully realize the capabilities of this sustainable adsorbent coating material. This can be achieved by tuning the surface area by modification of the NFLN, optimization of the particle size of the biocarbon coating, expanding the range of dye concentrations and selection of different dyes. Although results indicated an improvement in the NR film composite application, there is also significant room for further optimization through the optimization of the particle size, filler loading, curing procedures and selection of different rubbers.

References

1. Geyer, R., Jambeck, J. R. & Law, K. L. Production, use, and fate of all plastics ever made. *Sci. Adv.* **3**, e1700782 (2017).

2. Jubinville, D., Esmizadeh, E., Saikrishnan, S., Tzoganakis, C. & Mekonnen, T. A comprehensive review on global production and recycling methods of polyolefin (PO) based products and their post-recycling applications. *Sustain. Mater. Technol.* e00188 (2020).

3. Jardin, J. M., Zhang, Z., Hu, G., Tam, K. C. & Mekonnen, T. H. Reinforcement of rubber nanocomposite thin sheets by percolation of pristine cellulose nanocrystals. *Int. J. Biol. Macromol.* **152**, 428–436 (2020).

4. Trinh, B. M. & Mekonnen, T. Hydrophobic esterification of cellulose nanocrystals for epoxy reinforcement. *Polymer (Guildf).* **155**, 64–74 (2018).

5. Kai, D. *et al.* Towards lignin-based functional materials in a sustainable world. *Green Chem.* **18**, 1175–1200 (2016).

6. Ogunsona, E., Ojogbo, E. & Mekonnen, T. Advanced material applications of starch and its derivatives. *Eur. Polym. J.* **108**, 570–581 (2018).

7. Smolarski, N. High-Value Opportunities for Lignin: Unlocking its Potential Lignin potential. *Frost & Sullivan* **1**, 1–15 (2012).

8. Lora, J. H. & Glasser, W. G. Recent industrial applications of lignin: A sustainable alternative to nonrenewable materials. *J. Polym. Environ.* **10**, 39–48 (2002).

9. Bajwa, D. S., Pourhashem, G., Ullah, A. H. & Bajwa, S. G. A concise review of current lignin production, applications, products and their environment impact. *Ind. Crops Prod.* **139**, 111526 (2019).

10. Collard, F. X. & Blin, J. A review on pyrolysis of biomass constituents: Mechanisms and composition of the products obtained from the conversion of cellulose, hemicelluloses and lignin. *Renew. Sustain. Energy Rev.* **38**, 594–608 (2014).

11. Babeł, K. & Jurewicz, K. KOH activated lignin based nanostructured carbon exhibiting high hydrogen electrosorption. *Carbon N. Y.* **46**, 1948–1956 (2008).

12. Snowdon, M. R., Mohanty, A. K. & Misra, M. A study of carbonized lignin as an alternative to carbon black. *ACS Sustain. Chem. Eng.* **2**, 1257–1263 (2014).

13. Jiang, C. *et al.* Converting waste lignin into nano-biochar as a renewable substitute of carbon black for reinforcing styrene-butadiene rubber. *Waste Manag.* **102**, 732–742 (2020).

14. Suhas, Carrott, P. J. M. & Ribeiro Carrott, M. M. L. Lignin - from natural adsorbent to activated carbon: A review. *Bioresour. Technol.* **98**, 2301–2312 (2007).

15. Li, J., Li, Y., Wu, Y. & Zheng, M. A comparison of biochars from lignin, cellulose and wood as the sorbent to an aromatic pollutant. *J. Hazard. Mater.* **280**, 450–457 (2014).

16. Sarkanen, K. V. & Ludwig, C. H. *Lignins: occurrence, formation, structure and reactions*,. (Wiley-Interscience, 1971).

17. Dorrestijn, E., Laarhoven, L. J. J., Arends, I. W. C. E. & Mulder, P. Occurrence and reactivity of phenoxyl linkages in lignin and low rank coal. *J. Anal. Appl. Pyrolysis* **54**, 153–192 (2000).

18. Ralph, J. *et al.* Lignins: Natural polymers from oxidative coupling of 4-hydroxyphenyl-propanoids. *Phytochem. Rev.* **3**, 29–60 (2004).

19. Boerjan, W., Ralph, J. & Baucher, M. Lignin Biosynthesis. *Annu. Rev. Plant Biol.* **54**, 519–546 (2003).

20. Mottiar, Y., Vanholme, R., Boerjan, W., Ralph, J. & Mansfield, S. D. Designer lignins: Harnessing the plasticity of lignification. *Curr. Opin. Biotechnol.* **37**, 190–200 (2016).

21. Zhao, Q. *et al.* LACCASE is necessary and nonredundant with PEROXIDASE for lignin polymerization during vascular development in Arabidopsis. *Plant Cell* **25**, 3976–3987 (2013).

22. Russell, W. R., Forrester, A. R., Chesson, A. & Burkitt, M. J. Oxidative coupling during lignin polymerization is determined by unpaired electron delocalization within parent phenylpropanoid radicals. *Arch. Biochem. Biophys.* **332**, 357–366 (1996).

23. Tobimatsu, Y. & Schuetz, M. Lignin polymerization: how do plants manage the chemistry so well? *Curr. Opin. Biotechnol.* **56**, 75–81 (2019).

24. Davin, L. B. *et al.* Dissection of lignin macromolecular configuration and assembly: comparison to related biochemical processes in allyl/propenyl phenol and lignan biosynthesis. *Nat. Prod. Rep.* **25**, 1015–1090 (2008).

25. Bjørsvik, H. R. & Liguori, L. Organic processes to pharmaceutical chemicals based on fine chemicals from lignosulfonates. *Org. Process Res. Dev.* **6**, 279–290 (2002).

26. Parthasarathi, R., Romero, R. A., Redondo, A. & Gnanakaran, S. Theoretical study of the remarkably diverse linkages in lignin. *J. Phys. Chem. Lett.* **2**, 2660–2666 (2011).

27. Diop, A., Jradi, K., Daneault, C. & Montplaisir, D. Kraft lignin depolymerization in an ionic liquid without a catalyst. *BioResources* **10**, 4933–4946 (2015).

28. Mansouri, N. E. El & Salvadó, J. Structural characterization of technical lignins for the production of adhesives: Application to lignosulfonate, kraft, soda-anthraquinone, organosolv and ethanol process lignins. *Ind. Crops Prod.* **24**, 8–16 (2006).

29. Sixta, H. & Schild, G. a New Generation Kraft Process. *Lenzinger Berichte* **87**, 26–37 (2009).

30. Kim, S. & Holtzapple, M. T. Delignification kinetics of corn stover in lime pretreatment. *Bioresour. Technol.* **97**, 778–785 (2006).

31. Gierer, J. Chemical aspects of kraft pulping. *Wood Sci. Technol.* **14**, 241–266 (1980).

32. Matsushita, Y. Conversion of technical lignins to functional materials with retained

polymeric properties. *J. Wood Sci.* **61**, 230–250 (2015).

33. Xu, F., Sun, J. X., Sun, R., Fowler, P. & Baird, M. S. Comparative study of organosolv lignins from wheat straw. *Ind. Crops Prod.* **23**, 180–193 (2006).

34. Vishtal, A. G. & Kraslawski, A. Challenges in industrial applications of technical lignins. *BioResources* **6**, 3547–3568 (2011).

35. Pouteau, C., Dole, P., Cathala, B., Averous, L. & Boquillon, N. Antioxidant properties of lignin in polypropylene. *Polym. Degrad. Stab.* **81**, 9–18 (2003).

36. Ochsner, A; da Silva, Lucas; Altenbach, H. Advances in Natural Polymers. *Adv. Struct. Mater.* **18**, 424 (2013).

37. Richter, A. P. *et al.* An environmentally benign antimicrobial nanoparticle based on a silver-infused lignin core. *Nat. Nanotechnol.* **10**, 817–823 (2015).

38. Nada, A. M. A., El-Diwany, A. I. & Elshafei, A. M. Infrared and antimicrobial studies on different lignins. *Acta Biotechnol.* **9**, 295–298 (1989).

39. Leschine, S. B. Cellulose degradation in anaerobic environments. *Annu. Rev. Microbiol.* **49**, 399–426 (1995).

40. Pérez, J., Muñoz-Dorado, J., De La Rubia, T. & Martínez, J. Biodegradation and biological treatments of cellulose, hemicellulose and lignin: An overview. *Int. Microbiol.* **5**, 53–63 (2002).

41. Dessbesell, L., Paleologou, M., Leitch, M., Pulkki, R. & Xu, C. (Charles). Global lignin supply overview and kraft lignin potential as an alternative for petroleum-based polymers. *Renew. Sustain. Energy Rev.* **123**, 109768 (2020).

42. Aro, T. & Fatehi, P. Production and Application of Lignosulfonates and Sulfonated Lignin. *ChemSusChem* **10**, 1861–1877 (2017).

43. Hocking, M. B. Vanillin: synthetic flavoring from spent sulfite liquor. *J. Chem. Educ.* **74**, 1055 (1997).

44. Demuner, I. F., Colodette, J. L., Demuner, A. J. & Jardim, C. M. Biorefinery review: Wide-reaching products through kraft lignin. *BioResources* **14**, 7543–7581 (2019).

45. Souto, F., Calado, V. & Pereira, N. Lignin-based carbon fiber: A current overview. *Mater. Res. Express* **5**, 72001 (2018).

46. Nair, S. S. *et al.* High shear homogenization of lignin to nanolignin and thermal stability of nanolignin-polyvinyl alcohol blends. *ChemSusChem* **7**, 3513–3520 (2014).

47. Gilca, I. A., Popa, V. I. & Crestini, C. Obtaining lignin nanoparticles by sonication. *Ultrason. Sonochem.* **23**, 369–375 (2015).

48. Frangville, C. *et al.* Fabrication of environmentally biodegradable lignin nanoparticles. *ChemPhysChem* **13**, 4235–4243 (2012).

49. Lievonen, M. *et al.* A simple process for lignin nanoparticle preparation. *Green Chem.* **18**, 1416–1422 (2016).

50. Richter, A. P. *et al.* Synthesis and characterization of biodegradable lignin nanoparticles with tunable surface properties. *Langmuir* **32**, 6468–6477 (2016).

51. Myint, A. A. *et al.* One pot synthesis of environmentally friendly lignin nanoparticles with compressed liquid carbon dioxide as an antisolvent. *Green Chem.* **18**, 2129–2146 (2016).

52. Suslick, K. S., Hammerton, D. A. & Cline, R. E. The Sonochemical Hot Spot. *J. Am. Chem. Soc.* **108**, 5641–5642 (1986).

53. Wu, C., Liu, X., Wei, D., Fan, J. & Wang, L. Photosonochemical degradation of phenol in water. *Water Res.* **35**, 3927–3933 (2001).

54. Leonelli, C. & Mason, T. J. Microwave and ultrasonic processing: Now a realistic option for industry. *Chem. Eng. Process. Process Intensif.* **49**, 885–900 (2010).

55. Seino, T. *et al.* ESR studies of radicals generated by ultrasonic irradiation of lignin solution. An application of the spin trapping method. *Wood Sci. Technol.* **35**, 97–106 (2001).

56. Medalia, A. I. & Richards, L. W. Tinting strength of carbon black. *J. Colloid Interface Sci.* **40**, 233–252 (1972).

57. Ogunsona, E. O., Misra, M. & Mohanty, A. K. Influence of epoxidized natural rubber on the phase structure and toughening behavior of biocarbon reinforced nylon 6 biocomposites. *RSC Adv.* **7**, 8727–8739 (2017).

58. Ogunsona, E. O., Codou, A., Misra, M. & Mohanty, A. K. Thermally stable pyrolytic biocarbon as an effective and sustainable reinforcing filler for polyamide bio-composites fabrication. *J. Polym. Environ.* **26**, 3574–3589 (2018).

59. Pantea, D., Darmstadt, H., Kaliaguine, S., Sümmchen, L. & Roy, C. Electrical conductivity of thermal carbon blacks: Influence of surface chemistry. *Carbon N. Y.* **39**, 1147–1158 (2001).

60. Zhang, J., Feng, S. & Ma, Q. Kinetics of the thermal degradation and thermal stability of conductive silicone rubber filled with conductive carbon black. *J. Appl. Polym. Sci.* **89**, 1548–1554 (2003).

61. Wen, X. *et al.* Thermal and flammability properties of polypropylene/carbon black nanocomposites. *Polym. Degrad. Stab.* **97**, 793–801 (2012).

62. *Carbon Black Market Size, Share & Trends Analysis Report By Application (Tires, High-performance Coatings, Plastics), By Region (North America, Middle East & Africa, Asia Pacific, Europe), And Segment Forecasts, 2019 - 2025*. (2019).

63. Donnet, J.-B. *Carbon black: science and technology*. (CRC Press, 1993).

64. Long, C. M., Nascarella, M. A. & Valberg, P. A. Carbon black vs. black carbon and other airborne materials containing elemental carbon: Physical and chemical distinctions. *Environ. Pollut.* **181**, 271–286 (2013).

65. Amornwachirabodee, K. *et al.* Oxidized Carbon Black: Preparation, Characterization and Application in Antibody Delivery across Cell Membrane. *Sci. Rep.* **8**, 2489 (2018).

66. Watson, A. Y. & Valberg, P. A. Carbon black and soot: Two different substances. *Am. Ind. Hyg. Assoc. J.* **62**, 218–228 (2001).

67. Pantea, D., Darmstadt, H., Kaliaguine, S. & Roy, C. Electrical conductivity of conductive carbon blacks: Influence of surface chemistry and topology. *Appl. Surf. Sci.* **217**, 181–193 (2003).

68. Nowak, Z. T. Reinforcement of Rubber By Carbon Black. in *Properties of polymers* 21–68 (Springer, 1984).

69. Ren, W. & Cheng, H. M. The global growth of graphene. *Nat. Nanotechnol.* **9**, 726–730 (2014).

70. Ogunsona, E. O., Grovu, T. & Mekonnen, T. H. Fabrication of nano-structured graphene oxide-like few-layer sheets from biocarbon via a green process. *Sustain. Mater. Technol.* **26**, e00208 (2020).

71. El-Naggar, A. *et al.* Biochar application to low fertility soils: A review of current status, and future prospects. *Geoderma* **337**, 536–554 (2019).

72. Ahmed, M. J., Okoye, P. U., Hummadi, E. H. & Hameed, B. H. High-performance porous biochar from the pyrolysis of natural and renewable seaweed (Gelidiella acerosa) and its application for the adsorption of methylene blue. *Bioresour. Technol.* **278**, 159–164 (2019).

73. Chang, B. P., Mohanty, A. K. & Misra, M. Sustainable biocarbon as an alternative of traditional fillers for poly(butylene terephthalate)-based composites: Thermo-oxidative aging and durability. *J. Appl. Polym. Sci.* **136**, 47722 (2019).

74. Lehmann, J. & Stephen, J. *Biochar for Environmental Management: Science, Technology and Implementation*. *Science And Technology* **1**, (Routledge, 2015).

75. Kwapinski, W. *et al.* Biochar from biomass and waste. *Waste and Biomass Valorization* **1**, 177–189 (2010).

76. Ding, G., Wang, B., Chen, L. & Zhao, S. Simultaneous adsorption of methyl red and methylene blue onto biochar and an equilibrium modeling at high concentration. *Chemosphere* **163**, 283–289 (2016).

77. Hassan, A. F., Abdel-Mohsen, A. M. & Fouda, M. M. G. Comparative study of calcium alginate, activated carbon, and their composite beads on methylene blue adsorption. *Carbohydr. Polym.* **102**, 192–198 (2014).

78. Li, Y. *et al.* Comparative study of methylene blue dye adsorption onto activated carbon, graphene oxide, and carbon nanotubes. *Chem. Eng. Res. Des.* **91**, 361–368 (2013).

79. Cheng, M. *et al.* Combined biological removal of methylene blue from aqueous solutions using rice straw and Phanerochaete chrysosporium. *Appl. Microbiol. Biotechnol.* **99**, 5247–5256 (2015).

80. Li, Q. *et al.* Filtration and adsorption properties of porous calcium alginate membrane for methylene blue removal from water. *Chem. Eng. J.* **316**, 623–630 (2017).

81. Jing, H. P., Wang, C. C., Zhang, Y. W., Wang, P. & Li, R. Photocatalytic degradation of methylene blue in ZIF-8. *RSC Adv.* **4**, 54454–54462 (2014).

82. Rafatullah, M., Sulaiman, O., Hashim, R. & Ahmad, A. Adsorption of methylene blue on low-cost adsorbents: A review. *J. Hazard. Mater.* **177**, 70–80 (2010).

83. Lefebvre, L., Agusti, G., Bouzeggane, A. & Edouard, D. Adsorption of dye with carbon media supported on polyurethane open cell foam. *Catal. Today* **301**, 98–103 (2018).

84. Singh, V. P. & Vaish, R. Candle soot coated polyurethane foam as an adsorbent for removal of organic pollutants from water. *Eur. Phys. J. Plus* **134**, 1–10 (2019).

85. Agrawal, A., Kaur, R. & Walia, R. S. PU foam derived from renewable sources: Perspective on properties enhancement: An overview. *Eur. Polym. J.* **95**, 255–274 (2017).

86. Bergamonti, L., Taurino, R., Cattani, L., Ferretti, D. & Bondioli, F. Lightweight hybrid organic-inorganic geopolymers obtained using polyurethane waste. *Constr. Build. Mater.* **185**, 285–292 (2018).

87. Rose, K. & Steinbüchel, A. Biodegradation of natural rubber and related compounds: Recent insights into a hardly understood catabolic capability of microorganisms. *Appl. Environ. Microbiol.* **71**, 2803–2812 (2005).

88. Eslami, H., Tzoganakis, C. & Mekonnen, T. H. Constructing pristine and modified cellulose nanocrystals based cured polychloroprene nanocomposite films for dipped goods application. *Compos. Part C Open Access* **1**, 100009 (2020).

89. George, S. C., Rajan, R., Aprem, A. S., Thomas, S. & Kim, S. S. The fabrication and properties of natural rubber-clay nanocomposites. *Polym. Test.* **51**, 165–173 (2016).

90. Peng, Z., Feng, C., Luo, Y., Li, Y. & Kong, L. X. Self-assembled natural rubber/multi-walled carbon nanotube composites using latex compounding techniques. *Carbon N. Y.* **48**, 4497–4503 (2010).

91. Bokobza, L. Multiwall carbon nanotube-filled natural rubber: Electrical and mechanical properties. *Express Polym. Lett.* **6**, 213–223 (2012).

92. Anand K., A., Jose T., S., Alex, R. & Joseph, R. Natural rubber-carbon nanotube composites through latex compounding. *Int. J. Polym. Mater. Polym. Biomater.* **59**, 33–44 (2010).

93. Mao, Y. *et al.* High performance graphene oxide based rubber composites. *Sci. Rep.* **3**, 2508 (2013).

94. Zhang, Y. *et al.* The properties of rice bran carbon/nitrile-butadiene rubber composites fabricated by latex compounding method. *Polym. Compos.* **39**, E687–E696 (2018).

95. Peterson, S. C. Silica-Milled Paulownia Biochar as Partial Replacement of Carbon Black Filler in Natural Rubber. *Journal of Composites Science* **3**, 107 (2019).

96. Dominic C.D., M. *et al.* Chitin nanowhiskers from shrimp shell waste as green filler in acrylonitrile-butadiene rubber: Processing and performance properties. *Carbohydr. Polym.* **245**, 116505 (2020).

97. Dominic, M. *et al.* Green tire technology: Effect of rice husk derived nanocellulose (RHNC) in replacing carbon black (CB) in natural rubber (NR) compounding. *Carbohydr. Polym.* **230**, 115620 (2020).

98. Myllytie, P., Misra, M. & Mohanty, A. K. Carbonized Lignin as Sustainable Filler in Biobased Poly(trimethylene terephthalate) Polymer for Injection Molding Applications. *ACS Sustain. Chem. Eng.* **4**, 102–110 (2016).

99. Chen, F. *et al.* Facile preparation of cross-linked lignin for efficient adsorption of dyes and heavy metal ions. *React. Funct. Polym.* **143**, 104336 (2019).

100. Gonugunta, P., Vivekanandhan, S., Mohanty, A. K. & Misra, M. A Study on Synthesis and Characterization of Biobased Carbon Nanoparticles from Lignin. *World J. Nano Sci. Eng.* **02**, 148–153 (2012).

101. Baker, D. A. & Rials, T. G. Recent advances in low-cost carbon fiber manufacture from lignin. *J. Appl. Polym. Sci.* **130**, 713–728 (2013).

102. Das, S. Life cycle assessment of carbon fiber-reinforced polymer composites. *Int. J. Life Cycle Assess.* **16**, 268–282 (2011).

103. Neves, D., Thunman, H., Matos, A., Tarelho, L. & Gómez-Barea, A. Characterization and prediction of biomass pyrolysis products. *Prog. Energy Combust. Sci.* **37**, 611–630 (2011).

104. Ferrari, A. C. *et al.* Raman spectrum of graphene and graphene layers. *Phys. Rev. Lett.* **97**, 187401 (2006).

105. Goyal, H. B., Seal, D. & Saxena, R. C. Bio-fuels from thermochemical conversion of renewable resources: A review. *Renew. Sustain. Energy Rev.* **12**, 504–517 (2008).

106. Dall'Ora, M., Jensen, P. A. & Jensen, A. D. Suspension Combustion of Wood: Influence of Pyrolysis Conditions on Char Yield, Morphology, and Reactivity. *Energy & Fuels* **22**, 2955–2962 (2008).

107. Brunner, P. H. & Roberts, P. V. The significance of heating rate on char yield and char properties in the pyrolysis of cellulose. *Carbon N. Y.* **18**, 217–224 (1980).

108. Alongi, J., Camino, G. & Malucelli, G. Heating rate effect on char yield from cotton, poly(ethylene terephthalate) and blend fabrics. *Carbohydr. Polym.* **92**, 1327–1334 (2013).

109. Ferdous, D., Dalai, A. K., Bej, S. K., Thring, R. W. & Bakhshi, N. N. Production of H2 and medium Btu gas via pyrolysis of lignins in a fixed-bed reactor. *Fuel Process. Technol.* **70**, 9–26 (2001).

110. Li, C. *et al.* Impact of heating rates on the evolution of function groups of the biochar from lignin pyrolysis. *J. Anal. Appl. Pyrolysis* **155**, 105031 (2021).

111. Yean, W. Q. & Goring, D. A. I. The molecular weight of a sodium lignosulfonate in dimethylsulfoxide and in aqueous 0.1M sodium chlorine. *J. Appl. Polym. Sci.* **14**, 1115–1120 (1970).

112. Puskás, I., Szemjonov, A., Fenyvesi, É., Malanga, M. & Szente, L. Aspects of determining

the molecular weight of cyclodextrin polymers and oligomers by static light scattering. *Carbohydr. Polym.* **94**, 124–128 (2013).

113. Sharma, R. K. *et al.* Characterization of chars from pyrolysis of lignin. *Fuel* **83**, 1469–1482 (2004).

114. Zhao, J. *et al.* Thermal degradation of softwood lignin and hardwood lignin by TG-FTIR and Py-GC/MS. *Polym. Degrad. Stab.* **108**, 133–138 (2014).

115. Jakab, E., Faix, O., Till, F. & Székely, T. Thermogravimetry/mass spectrometry study of six lignins within the scope of an international round robin test. *J. Anal. Appl. Pyrolysis* **35**, 167–179 (1995).

116. Melkior, T. *et al.* NMR analysis of the transformation of wood constituents by torrefaction. *Fuel* **92**, 271–280 (2012).

117. Asmadi, M., Kawamoto, H. & Saka, S. Gas- and solid/liquid-phase reactions during pyrolysis of softwood and hardwood lignins. *J. Anal. Appl. Pyrolysis* **92**, 417–425 (2011).

118. Bridgwater, A. V. Principles and practice of biomass fast pyrolysis processes for liquids. *J. Anal. Appl. Pyrolysis* **51**, 3–22 (1999).

119. Ruiz-Rosas, R. *et al.* The production of submicron diameter carbon fibers by the electrospinning of lignin. *Carbon N. Y.* **48**, 696–705 (2010).

120. Gonzalez-Serrano, E., Cordero, T., Rodríguez-Mirasol, J. & Rodríguez, J. J. Development of Porosity upon Chemical Activation of Kraft Lignin with ZnCl2. *Ind. Eng. Chem. Res.* **36**, 4832–4838 (1997).

121. van Loon, W. M. G. M., Boon, J. J. & de Groot, B. Quantitative Analysis of Sulfonic Acid Groups in Macromolecular Lignosulfonic Acids and Aquatic Humic Substances by Temperature-Resolved Pyrolysis-Mass Spectrometry. *Environ. Sci. Technol.* **27**, 2387–2396 (1993).

122. Watt, W. *Polymeric carbons — Carbon fibre, glass and char*. *Polymer* **18**, (Cambridge University Press, 1977).

123. Rodríguez-Reinoso, F. & Molina-Sabio, M. Activated carbons from lignocellulosic materials by chemical and/or physical activation: an overview. *Carbon N. Y.* **30**, 1111–1118 (1992).

124. Kim, P. *et al.* Surface functionality and carbon structures in lignocellulosic-derived biochars produced by fast pyrolysis. *Energy and Fuels* **25**, 4693–4703 (2011).

125. Mészáros, E. *et al.* Do all carbonized charcoals have the same chemical structure? 1. Implications of thermogravimetry-mass spectrometry measurements. *Ind. Eng. Chem. Res.* **46**, 5943–5953 (2007).

126. Hu, C. *et al.* Raman spectroscopy study of the transformation of the carbonaceous skeleton of a polymer-based nanoporous carbon along the thermal annealing pathway. *Carbon N. Y.* **85**, 147–158 (2015).

127. Pang, J. *et al.* Facile and sustainable synthesis of sodium lignosulfonate derived

hierarchical porous carbons for supercapacitors with high volumetric energy densities. *Green Chem.* **19**, 3916–3926 (2017).

128. Nandiwale, K. Y., Danby, A. M., Ramanathan, A., Chaudhari, R. V. & Subramaniam, B. Zirconium-Incorporated Mesoporous Silicates Show Remarkable Lignin Depolymerization Activity. *ACS Sustain. Chem. Eng.* **5**, 7155–7164 (2017).

129. Deepa, A. K. & Dhepe, P. L. Lignin Depolymerization into Aromatic Monomers over Solid Acid Catalysts. *ACS Catal.* **5**, 365–379 (2015).

130. Liu, Y. *et al.* A sustainable route for the preparation of activated carbon and silica from rice husk ash. *J. Hazard. Mater.* **186**, 1314–1319 (2011).

131. Addoun, A., Dentzer, J. & Ehrburger, P. Porosity of carbons obtained by chemical activation: Effect of the nature of the alkaline carbonates. *Carbon N. Y.* **40**, 1140–1143 (2002).

132. Xu, J. *et al.* Raman spectroscopy of biochar from the pyrolysis of three typical Chinese biomasses: A novel method for rapidly evaluating the biochar property. *Energy* **202**, 117644 (2020).

133. Hauptman, N., Vesel, A., Ivanovski, V. & Gunde, M. K. Electrical conductivity of carbon black pigments. *Dye. Pigment.* **95**, 1–7 (2012).

134. Ma, Z. *et al.* Evolution of the chemical composition, functional group, pore structure and crystallographic structure of bio-char from palm kernel shell pyrolysis under different temperatures. *J. Anal. Appl. Pyrolysis* **127**, 350–359 (2017).

135. TUINSTRA F & KOENIG JL. Raman Spectrum of Graphite. *J. Chem. Phys.* **53**, 1126–1130 (1970).

136. Paris, O., Zollfrank, C. & Zickler, G. A. Decomposition and carbonisation of wood biopolymers - A microstructural study of softwood pyrolysis. *Carbon N. Y.* **43**, 53–66 (2005).

137. Ribeiro-Soares, J. *et al.* Structural analysis of polycrystalline graphene systems by Raman spectroscopy. *Carbon N. Y.* **95**, 646–652 (2015).

138. Zhao, Y., Feng, D., Zhang, Y., Huang, Y. & Sun, S. Effect of pyrolysis temperature on char structure and chemical speciation of alkali and alkaline earth metallic species in biochar. *Fuel Process. Technol.* **141**, 54–60 (2016).

139. Giorcelli, M. & Bartoli, M. Development of coffee biochar filler for the production of electrical conductive reinforced plastic. *Polymers (Basel).* **11**, 1–17 (2019).

140. Mendonça, F. G. de, Cunha, I. T. da, Soares, R. R., Tristão, J. C. & Lago, R. M. Tuning the surface properties of biochar by thermal treatment. *Bioresour. Technol.* **246**, 28–33 (2017).

141. Guizani, C., Haddad, K., Limousy, L. & Jeguirim, M. New insights on the structural evolution of biomass char upon pyrolysis as revealed by the Raman spectroscopy and elemental analysis. *Carbon N. Y.* **119**, 519–521 (2017).

142. Karaca, S., Gürses, A., Açikyildiz, M. & Ejder (Korucu), M. Adsorption of cationic dye from aqueous solutions by activated carbon. *Microporous Mesoporous Mater.* **115**, 376–382 (2008).

143. Sudaryanto, Y., Hartono, S. B., Irawaty, W., Hindarso, H. & Ismadji, S. High surface area activated carbon prepared from cassava peel by chemical activation. *Bioresour. Technol.* **97**, 734–739 (2006).